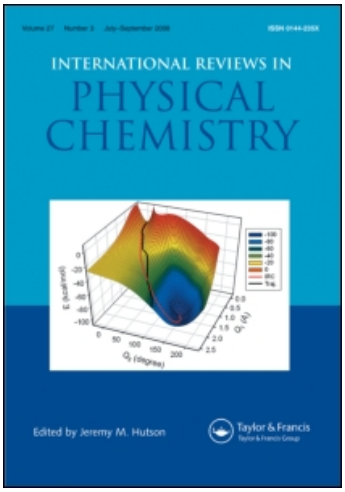

International Reviews in Physical Chemistry
Publication details, including instructions for authors and subscription information:
http://www.informaworld.com/smpp/title~content=t713724383

Structures, charge distributions, and dynamical properties of weakly bound complexes of aromatic molecules in their ground and electronically excited states

Cheolhwa Kang[a]; David W. Pratt[a]
[a] Department of Chemistry, University of Pittsburgh, Pittsburgh, PA 15260, USA

To cite this Article Kang, Cheolhwa and Pratt, David W.(2005) 'Structures, charge distributions, and dynamical properties of weakly bound complexes of aromatic molecules in their ground and electronically excited states', International Reviews in Physical Chemistry, 24: 1, 1 — 36
To link to this Article: DOI: 10.1080/01442350500161453
URL: http://dx.doi.org/10.1080/01442350500161453

International Reviews in Physical Chemistry,
Vol. 24, No. 1, January–March 2005, 1–36

Taylor & Francis
Taylor & Francis Group

Structures, charge distributions, and dynamical properties of weakly bound complexes of aromatic molecules in their ground and electronically excited states

CHEOLHWA KANG and DAVID W. PRATT*

Department of Chemistry, University of Pittsburgh, Pittsburgh, PA 15260, USA

(*Received 2 March 2005; in final form 28 April 2005*)

Described herein are the results of high-resolution electronic spectroscopy experiments on the weakly bound complexes of several aromatic molecules in the gas phase. The systems examined include *p*-difluorobenzene, indole, and 7-azaindole to which a single argon atom or a nitrogen or water molecule is attached. The experiments provide unique information about the structures of these complexes, their charge distributions, and their internal motions, including large-amplitude vibrations, internal rotations, and inversion-torsion motions. These properties change dramatically from one substrate to the next, as a consequence of changes in its symmetry, and when it is excited by light, as a consequence of changes in its electronic structure. Stark-effect experiments in the presence of applied electric fields probe these changes directly, providing for the first time values of the permanent and induced dipole moments of isolated molecules in different electronic states.

Contents

*Corresponding author. Email: pratt@pitt.edu

International Reviews in Physical Chemistry
ISSN 0144–235X print/ISSN 1366–591X online
http://www.tandf.co.uk/journals
DOI: 10.1080/01442350500161453

1. Introduction

Advances in science are often driven by advances in instrumentation. Our developing understanding of the forces between molecules is no exception. The pioneering work in this field was done by Levy and co-workers [1], who demonstrated that the use of supersonic jets to simplify the electronic spectra of large molecules led to the 'adventitious' formation of a wide variety of complexes held together by weak van der Waals forces and somewhat stronger hydrogen bonds. Performing these experiments with vibrational and rotational resolution, and at other frequencies (e.g. IR and microwave), gave exciting new information about the equilibrium geometries and dynamical properties of many new molecules whose existence in nature was demonstrated for the first time. Water aggregates like $(H_2O)_2$, $(H_2O)_3, \ldots, (H_2O)_n$ are a beautiful example, but there are many others [2–5]. This information, in turn, has fuelled the development of powerful new theoretical tools for calculating intermolecular potentials [6]. Predictions based on these calculations are likely to stimulate many further experiments, thereby 'completing' the scientific cycle of experiment, theory, and hypothesis in this new field.

Understanding the factors that contribute to the potential energy of interaction between two or more species is an important research objective. All encounters between atoms and molecules, whether reactive or unreactive, are (at least in the beginning) governed by such potentials. Of particular interest are the changes in the potentials that occur when two species approach each other, and how these changes depend upon angular coordinates. The 'induced fit' that characterizes the behaviour of many enzyme-substrate complexes in biology is representative of problems in this class. Beyond such molecular assemblies, the properties of collections of molecules in liquids, solutions, and solids also depend on their interactions at long range, and how the interaction between two species is affected by the presence of others (i.e. many-body effects).

Described here are the results of recent high-resolution electronic spectroscopy experiments on several weakly bound complexes of organic molecules. The substrates include *p*-difluorobenzene (*p*DFB), indole (IN), and 7-azaindole (7AI), see below:

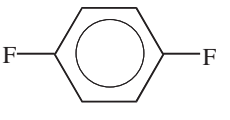

*p*DFB

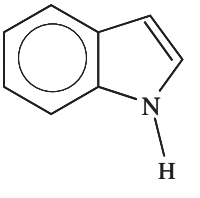

IN

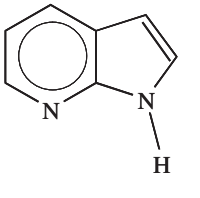

7AI

The complexing 'agents' include argon (Ar), nitrogen (N_2), and water (H_2O). We thus explore the properties of atomic, diatomic, and triatomic complexes of increasingly complex host molecules. Our experiments are rotationally resolved. Hence, we determine the equilibrium geometries of each complex in its electronic ground state. A particular focus is on how these geometries change when the substrate to which the atom or molecule is attached becomes more asymmetric. Similar information is obtained about the electronically excited state. In many cases, the geometry of the excited state is different from that of the ground state, owing to changes in the electron distribution of the substrate when it absorbs light. Van der Waals 'bonding' is entirely the result of electron correlation; such correlation, in turn, is often significantly enhanced in excited states, compared to ground states.

The second focus of this paper is on the permanent electric dipole moments of these complexes in their ground and electronically excited states. These have been measured for the first time using a newly developed Stark cell in our high-resolution apparatus, by means of which homogeneous electric fields may be applied to the sample. Two such studies will be described here, on 7AI-Ar and IN-H_2O. These studies give quantitative information about the changes in the charge distribution that are produced when a molecule absorbs light, thereby accounting for differences in the structures of the different complexes in their ground and electronically excited states. In the case of IN-H_2O, the Stark measurements also give information about induced dipole moments; i.e. the changes in the charge distribution of a substrate molecule that are produced when the complex is formed, a precursor to induced fits in biological systems.

The third and final focus of this paper is on the dynamical properties of weakly bound complexes in their ground and electronically excited states. The relatively weak interactions between closed shell molecules that are the hallmarks of such species gives rise to intermolecular bonds that are not rigid. As a result, Ar, N_2, and H_2O all undergo large-amplitude motions when they are attached to *p*DFB, IN, or 7AI. Additionally, in the case of N_2 and H_2O, the attached molecule undergoes other internal motions such as hindered rotation and inversion. Surprisingly, the observed high-resolution spectra are extraordinarily sensitive to these dynamics. Thus, properly interpreted, one can derive exquisitely detailed intermolecular potentials in both ground and electronically excited states from such data.

2. Experimental

Rotationally resolved electronic spectra were obtained using the CW molecular beam laser spectrometer that is described in detail elsewhere [7]; see figure 1. The clusters were generated by expanding a gas mixture of solute/solvent diluted with Ar (or He) carrier gas into a vacuum chamber. Different clusters require different conditions for their formation. The present conditions were as follows: (1) Ar complexes; flowing Ar carrier gas (~0.7 bar for 7AI, ~1.3 bar for indole); (2) N_2 complexes; seeded in a mixture of 10–15% N_2 in a He carrier gas (~0.7 bar for *p*DFB); (3) H_2O complexes; He carrier gas (~2.7 bar) was enriched with water vapour by passing the gas through a container holding water at room temperature. The substrate molecules were kept in a sample housing whose temperature was controlled to obtain a sufficient vapour

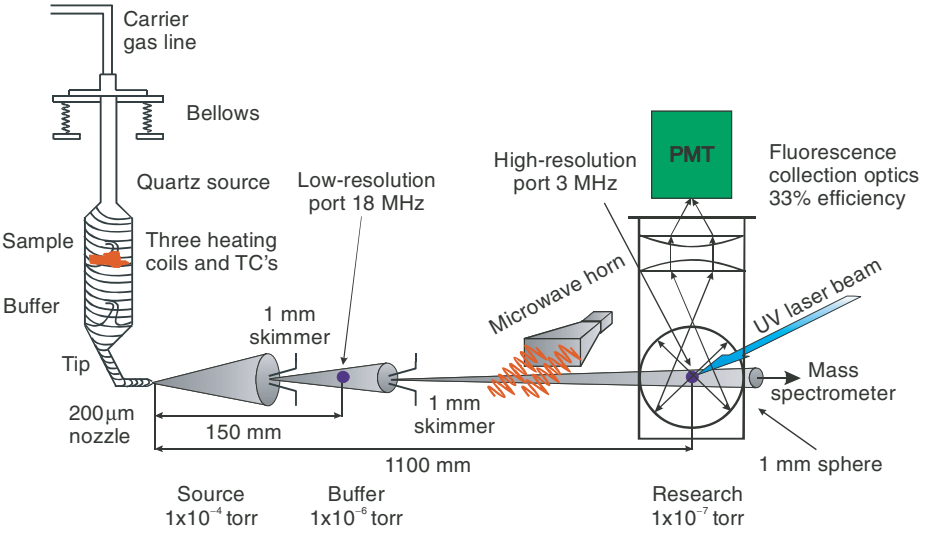

Figure 1. Overall layout of the high-resolution CW laser/molecular beam spectrometer.

pressure. To form a molecular beam, the expansion was skimmed 2 cm downstream of the nozzle with a 1 mm skimmer and crossed 13 cm further downstream by a continuous wave (CW) ring dye laser operating with a selected dye and intracavity frequency doubled in BBO, yielding 100–200 μW of ultraviolet radiation. Fluorescence was collected using spatially selective optics, detected by a photomultiplier tube and photon counting system, and processed by a computerized data acquisition system. Relative frequency calibrations of the spectra were performed using a near-confocal interferometer having a mode-matched FSR of 299.7520 ± 0.0005 MHz at the fundamental frequency of the dye laser. Absolute frequencies in the spectra were determined by comparison to transition frequencies in the electronic absorption spectrum of I_2 [8].

Homogeneous, static electric fields in the laser/molecule interaction region for the Stark-effect measurements were generated as follows. Two spherical mirrors were positioned above and below the intersection of the laser and molecular beams to collect the fluorescence. The top mirror has a focus at the intersection and the bottom mirror has a focus at a hole (2 mm) drilled in the centre of the top mirror. Two stainless steel wire grids were then placed inside these mirrors, separated by ~1 cm with ceramic spacers. Two power supplies were used to hold one grid at some positive voltage and the other at some negative voltage relative to a common ground. This experimental setup yields an electric field perpendicular to the polarization of the laser radiation and thus forces a selection rule of $\Delta M = \pm 1$. Electric field strengths were calibrated using the known value of μ_a in the ground state of aniline [9] and the combination-difference method of spectral assignment.

2.1. *Argon atom complexes*

2.1.1. *p*DFB-Ar. Our first example of the application of these techniques is taken from the literature. Figure 2 shows the rotationally resolved fluorescence excitation spectra of the 0_0^0 bands in the S_1–S_0 transitions of *p*DFB and its single-atom Ar complex

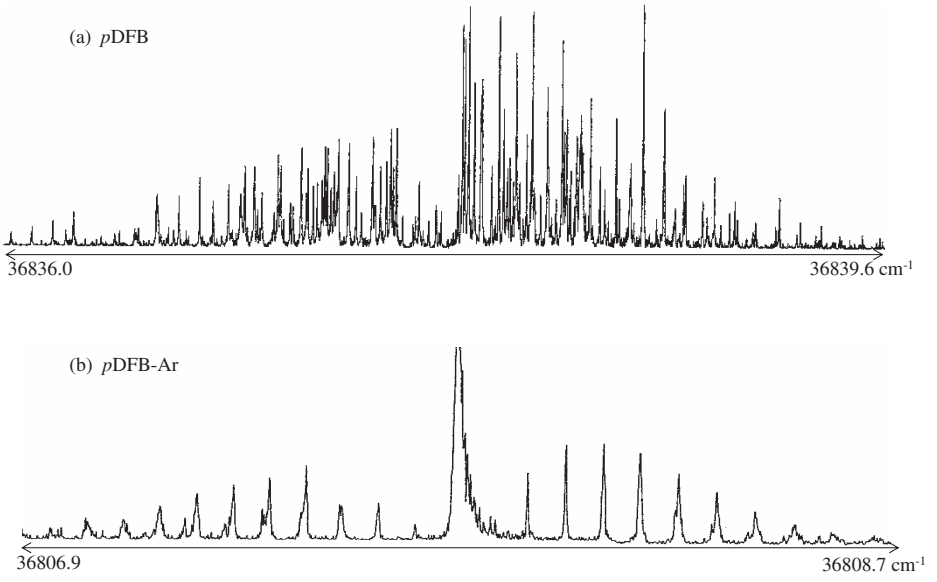

Figure 2. Rotationally resolved fluorescence excitation spectra of the origin bands in the S_1–S_0 transitions of (a) bare *p*-difluorobenzene at 36837.8 cm^{-1} and (b) the *p*-difluorobenzene-argon van der Waals complex at 36807.8 cm^{-1} [10].

*p*DFB-Ar obtained by Neusser and co-workers [10]. Now, the rotational motions of such large molecules are 'slow' on the time-scale of their vibrational motions (even the intermolecular ones!). Therefore, the high-resolution electronic spectroscopy experiment explores the *equilibrium* geometries of the two electronic states, averaged over their zero-point motions along all coordinates. This is the principal strength of eigenstate spectroscopy in the gas phase.

Information about these geometries is obtained in the first instance by fitting the experimental spectra with rigid rotor Hamiltonians for both states,

$$\hat{H} = AP_a^2 + BP_b^2 + CP_c^2 \tag{1}$$

Here, A, B, and C are the usual rotational constants, inversely related to the moments of inertia about each of the three principal axes (e.g. $A = h/8\pi^2\, c\, I_a$, etc.). (Later, centrifugal distortion constants can be included [11].) The fitting procedures that we use to fit such spectra are described elsewhere [12]. Suffice it to say here that a least-squares fit is performed on hundreds of lines, yielding rotational constants for both electronic states that are usually determined to precisions on the order of a few tenths of a MHz, substantially less than the single rovibronic linewidth of a few MHz. Additional parameters derived from these fits include the band origin frequency, the polarization of the band (i.e. the electronic TM orientation), and other terms that describe the strengths of couplings between other degrees of freedom and the rotational motion (*vide infra*).

Listed in table 1 are the values of the rotational constants of *p*DFB and *p*DFB-Ar in their S_0 and S_1 electronic states that were determined from fits of their high-resolution spectra by Sussman *et al*. [10]. Note, first, that the ground and excited state rotational

Table 1. Inertial parameters of *p*DFB and its Ar complex in their ground and excited electronic states [10].

State	Parameter	*p*DFB	*p*DFB-Ar
S_0	A, MHz	5639.1	1139.5
	B, MHz	1428.2	1029.7
	C, MHz	1139.5	695.5
	ΔI, uÅ^2	0.0	−207.7
S_1	A, MHz	5282.0 (3)	1129.0 (3)
	B, MHz	1435.1 (6)	1106.0 (3)
	C, MHz	1128.6 (6)	706.0 (9)
	ΔI, uÅ^2	−0.02	−188.7

constants of *p*DFB itself are significantly different. The *A* rotational constant decreases by 357.1 MHz, or 6.3%. This decrease signals a large change in geometry when *p*DFB absorbs light, which in turn demonstrates that its S_1 state has a significantly different electronic distribution from that of the S_0 state. Next, we note that the rotational constants of *p*DFB-Ar are very different from those of *p*DFB, reflecting the complex's larger mass. We also see that the *A* rotational constant of the complex is very nearly the same as the *C* rotational constant of the bare molecule. This indicates that the identities of the *a* and *c* inertial axes are interchanged on complex formation, and that the Ar atom lies above or below the aromatic plane in the equilibrium geometry of *p*DFB-Ar. In agreement with this, the polarizations of the two origin bands are different (cf. figure 2). And finally, we note that the S_0 and S_1 rotational constants of the complex also are different. *A* and *B* decrease, but *C* increases when the photon is absorbed, evidencing another difference in the geometries of the two electronic states of *p*DFB-Ar.

Quantitative information about the equilibrium geometries of *p*DFB-Ar in its two states can be obtained using Kraitchman's equations [13]. As shown in figure 3, attaching a mass *m* to a substrate molecule *M* with principal moments of inertia I_a, I_b, I_c changes its moments in a way that depends on the added mass *m* and its position in the inertial frame. Therefore, knowing its mass, one can determine the *a*, *b*, and *c* coordinates of Ar atom in the complex by comparing its rotational constants with those of the bare molecule. This is the Kraitchman procedure [13]. To be valid, it is only necessary that the geometry of the host molecule be unaffected by complex formation. Clearly, such an assumption must break down occasionally (for example, in the case of 'induced fits'), but this is not likely in weakly bound van der Waals complexes.

$$\begin{vmatrix} I_a & & \\ & I_b & \\ & & I_c \end{vmatrix} \xrightarrow[\text{at the point (x,y,z)}]{\text{Adding mass}} \begin{vmatrix} I_a+\mu(y^2+z^2) & -\mu xy & -\mu xz \\ -\mu xy & I_b+\mu(x^2+z^2) & -\mu yz \\ -\mu zx & -\mu yz & I_c+\mu(y^2+x^2) \end{vmatrix} = \begin{vmatrix} I'_a & & \\ & I'_b & \\ & & I'_c \end{vmatrix}$$

Bare molecule inertia tensor **Complex inertia tensor**

Figure 3. Kraitchman's equations.

Table 2. Centre-of-mass (COM) coordinates of the Ar atom in the principal axis frame of *p*DFB from Kraitchman's equations.

Coordinate (Å)	S_0	S_1
$\langle a^2\rangle^{1/2}$	0.0095 (27)	0.0350 (4)
$\langle b^2\rangle^{1/2}$	0.07 (2)	0.346 (4)
$\langle c^2\rangle^{1/2}$	3.5505 (5)	3.4827 (4)

Table 2 lists the COM coordinates of the Ar atom in *p*DFB-Ar that were determined in this way. First, we focus on the values of $|c|$, the out-of-plane displacement coordinate. The Ar atom is located at a distance of 3.55 Å above (or below) the aromatic plane in the S_0 state. The intermolecular potential energy surface is likely to be quite 'stiff' in this direction; hence, the value $|c| = 3.55$ Å is likely to be close to the equilibrium value. The value of $|c|$ decreases to 3.48 Å in the S_1 state, evidencing stronger binding in that state, a fact that is also evidenced by the redshift of the origin band of the complex relative to that of the bare molecule. A blueshifted origin band would indicate a less tightly bound Ar atom in the excited state. Thus, we conclude further that the S_1 wavefunction of *p*DFB is significantly more polarizable, leading to enhanced electron correlation (and tighter binding) in that state.

*p*DFB is a D_{2h} molecule; hence, we might expect the two in-plane coordinates, *a* and *b*, to be zero, in both states. This is not the case. The reason that these two coordinates are not zero is that the Ar atom undergoes large vibrational displacements along these coordinates, in both directions. Rotational constants are a measure of the r.m.s. displacements along these coordinates, not their average values (see below) [14].

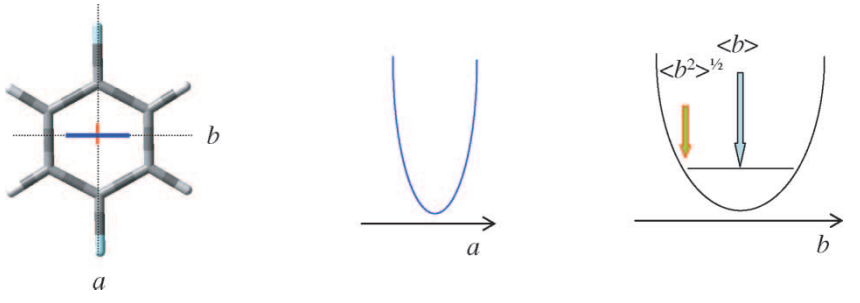

Thus, they are extremely sensitive to the detailed shape of the intermolecular potential along *a* and *b*. In this case, the large increase in $|b|$ in the S_1 state of *p*DFB-Ar is particularly striking; it is an order of magnitude large than $|a|$.

Figure 4 illustrates what we believe to be the explanation for this remarkable effect. Shown there is a difference density plot, indicating the regions of the molecule in which the π-electron density changes when *p*DFB absorbs light. These were calculated using the Gaussian 98 suite of programs [15]. A 6-31G* basis set was employed; the MP2 method was used for the S_0 state and the CIS method was used for the S_1 state. These calculations qualitatively reproduce the changes in the rotational constants that occur when the molecule absorbs light. These changes are a consequence of a quinoidal distortion of the ring. Thus, as figure 4 shows, there is a shift in π-electron

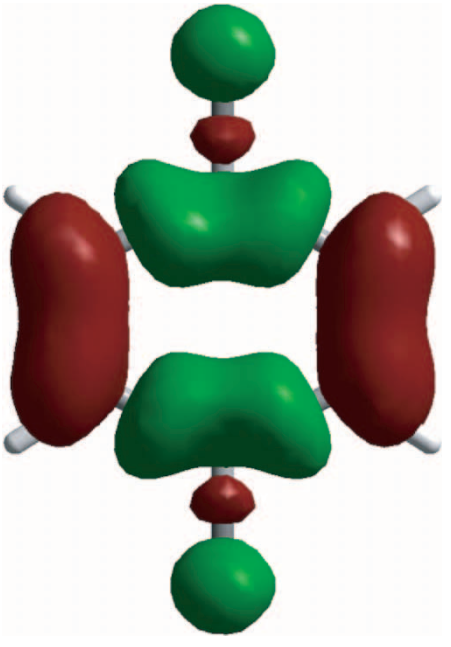

Figure 4. Electron density difference map for the S_1–S_0 transition of *p*-difluorobenzene. Red (black) contours indicate regions of electron gain, and green (grey) contours indicate regions of electron loss.

density from regions perpendicular to the C–F bonds to regions parallel to these bonds. As a result, this distribution is much more anisotropic in the S_1 state.

One measure of this anisotropy is the quadrupole moment of the charge distribution. Theoretical values of these are shown in table 3. Q_a and Q_b, though having different signs, are similar in magnitude in the S_0 state. Thus, the motion of the attached Ar atom should have more or less equal amplitudes in both directions. However, when the molecule is excited to its S_1 state, this distribution changes; $|Q_b|$ is much larger than $|Q_a|$. This leads to larger amplitude motions in directions perpendicular to a, and to larger vibrationally averaged values of $|b|$, compared to $|a|$. Thus illustrated, perhaps for the first time, is a significant dependence of the vibrational motion of the weakly bound Ar to the electronic distribution of the substrate to which it is attached.

Another measure of this anisotropy are the intermolecular vibrations. Bands involving excitation of the stretching and bending coordinates in S_1 *p*DFB-Ar also have been

Table 3. Quadrupole moments of *p*-difluorobenzene in its S_0 and S_1 electronic states, according to theory (MP2/CIS 6-31G**).

Quad. Mom.[a]	S_0	S_1
Q_a	−19.27	−9.64
Q_b	+19.18	+12.62
Q_c	+0.10	−2.97

[a]In units of Debye Ångstroms, in the inertial coordinate system of *p*DFB.

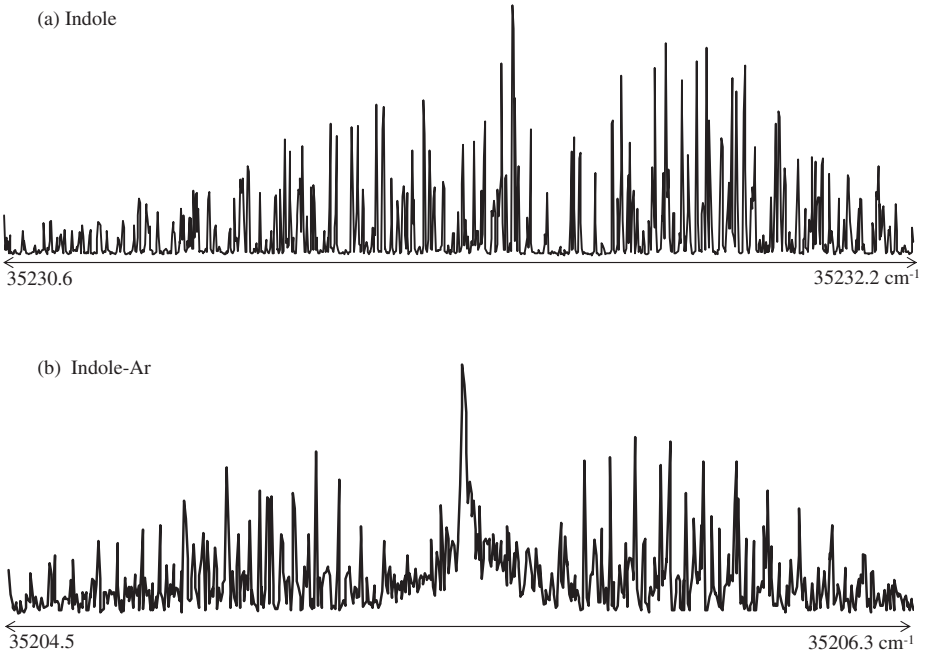

Figure 5. Rotationally resolved fluorescence excitation spectra near 284 nm of the origin bands in the S_1–S_0 transitions of (a) bare indole at 35 231 cm^{-1} and (b) the indole-argon van der Waals complex at 35 205 cm^{-1} [17].

measured at high resolution [16]. The long in-plane bend (motion parallel to *a*) is found at ~25 cm^{-1}, and the short in-plane bend (motion parallel to *b*) is found at ~34 cm^{-1}. The two modes also have very different rotational constants.

2.1.2. IN-Ar and 7AI-Ar. *p*DFB has fairly high symmetry. Therefore, it was of interest to learn how the properties of van der Waals complexes might be modified by making the substrate less symmetric. This was the purpose of our experiments on indole-Ar (IN-Ar) and 7-azaindole-Ar (7AI-Ar). Figure 5 compares the high-resolution spectrum of IN-Ar with that of indole itself [17]. The complex-induced change in the orientations of the inertial axes is immediately apparent. The hybrid band character of the origin band in the bare molecule (61.6% *a* and 38.4% *b*) is changed to 12% *a*, 47% *b*, and 41% *c* in IN-Ar. Beyond this, a rigorous fit of the spectrum (see figure 6) requires an additional assumption that inertial axis tilting occurs when the photon is absorbed.

'Axis tilting' refers to an interesting situation that can develop when the principal axes of the moment of inertia tensor in two different electronic states of a molecule do not coincide. This phenomenon was first detected in the electronic spectra of acetylene and other small molecules, and explained in a landmark paper by Hougen and Watson [18]. More recently, axis tilting has been detected in several large molecules [19]. Fundamentally, since the intensities in an electronic spectrum depend upon the

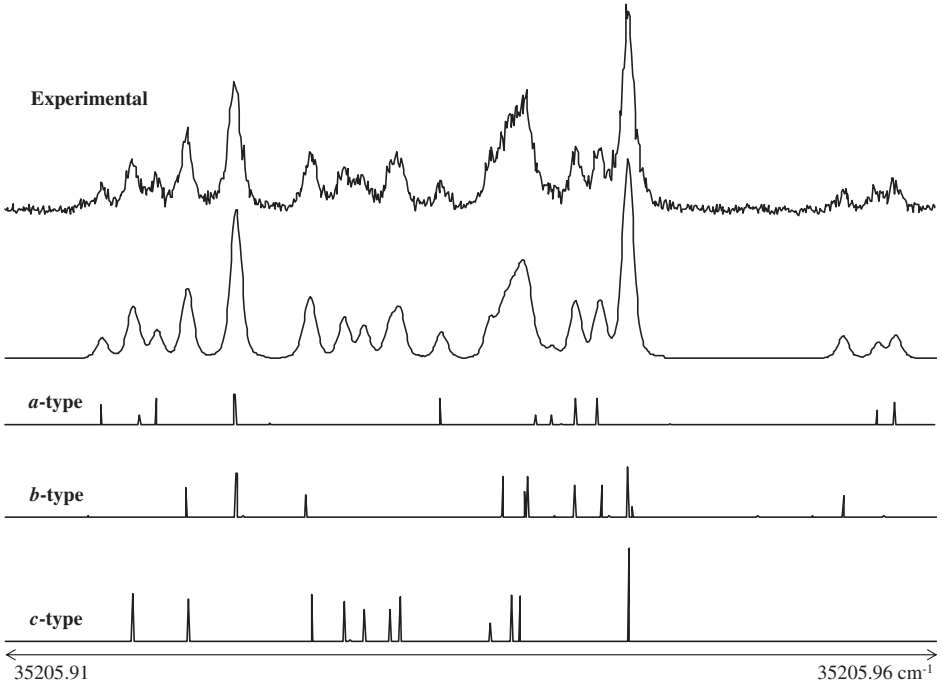

Figure 6. A portion of the high-resolution spectrum of indole-argon at full experimental resolution, extracted from the *R* branch. The top trace is the experimental spectrum. The second trace is the sum of the *a*-, *b*-, and *c*-type calculated spectra in the lower three traces, each of which has been convoluted with a 22 MHz FWHM Voigt lineshape profile (16 MHz Gaussian component and 8 MHz Lorentzian component) [17].

projection of the TM on the inertial axes, and since these projections change when axis tilting occurs, this can lead to anomalous intensities in a fully resolved spectrum. A full discussion of such 'quantum interference' effects and how they might be exploited is given elsewhere [20].

The axis tilting that occurs in IN-Ar is clearly a consequence of changes in electronic distribution that take place when the molecule absorbs light. Since the substrate itself is asymmetric, a change in that distribution results in a change in the equilibrium position of the Ar atom, not just in its vibrationally averaged coordinates. We therefore expected a similar result when we undertook a study of the similar molecule, 7AI-Ar. Figure 7 shows its high-resolution spectrum, which shows no evidence of axis tilting at all [21]. (As discussed elsewhere [20], quantum interference effects are most pronounced in a fully resolved spectrum when the band is a hybrid band. The 0_0^0 band of 7AI-Ar is a mainly *b*-type band, so large interference effects are not expected, in any event.) Apparently, either the equilibrium geometry of 7AI-Ar, or the change in that geometry which occurs when it absorbs light, is significantly different from that in IN-Ar.

Table 4 lists the COM coordinates of the Ar atom in the principal axis frames of indole (in the IN-Ar complex) and of 7AI (in the 7AI-Ar complex) that were determined from Kraitchman analyses of their corresponding spectra [17, 21]. (In this case, fits of the spectra of both IN-Ar and 7AI-Ar evidence significant centrifugal distortion

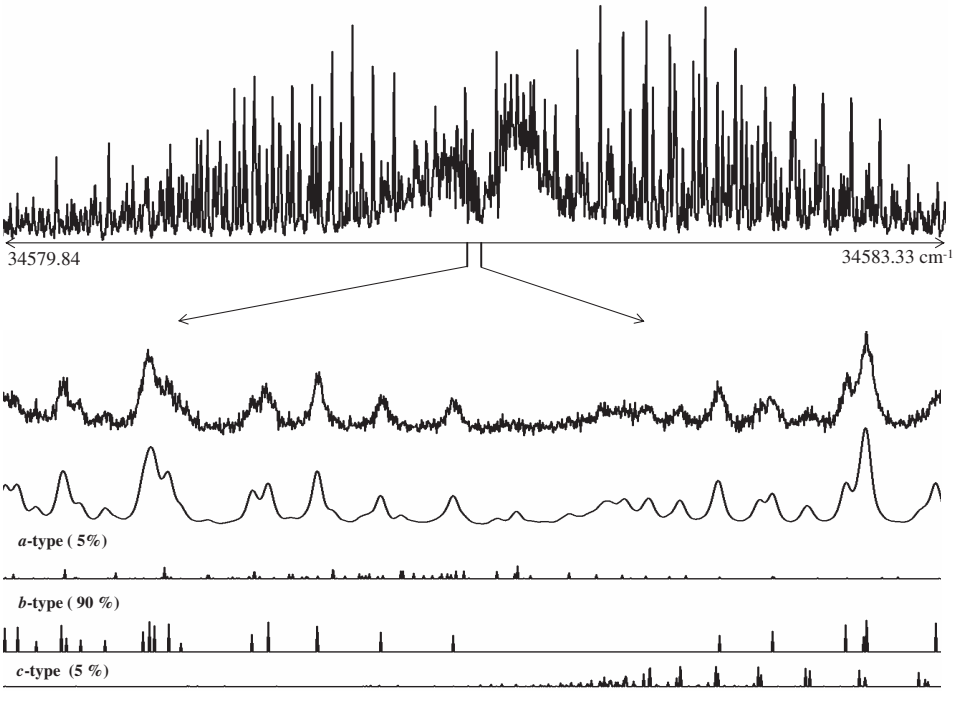

Figure 7. Rotationally resolved fluorescence excitation spectrum of the 7-azaindole-argon complex. The top trace shows the overall experimental spectrum. The bottom traces show a $\sim 0.1\,cm^{-1}$ portion of the experimental spectrum and two simulations, with and without a superimposed lineshape function. The individual *a*-, *b*-, and *c*-type contributions are also shown [21].

effects [23]. Corrections for these effects have been applied to the data in table 4.) Examining the results, we see that the Ar atom lies above (or below) the IN (7AI) plane at a distance of 3.43 Å (3.41 Å), slightly less than the corresponding distance in *p*DFB. The van der Waals 'bond' appears to be slightly stronger in the larger ring systems. This distance decreases by ~0.3 Å on absorption of light, again in accord with the redshifts of the Ar complex bands ($-26\,cm^{-1}$ in both IN and 7AI). But the most interesting data in this table are the in-plane coordinates, *a* and *b*. Both $|a|$ and $|b|$ are large in IN-Ar, and roughly equal in both electronic states. Their magnitudes decrease on S_1

Table 4. Comparison of the centre-of-mass (COM) coordinates in Å of the Ar atom in the principal axis frame of indole in the indole-Ar complex and of 7-azaindole in the 7-azaindole-Ar complex, as determined from a Kraitchman analysis.

State	Coordinate	Indole-Ar	7-Azaindole-Ar
S_0	$\|a\|$	0.411 (1)	0.088 (4)
	$\|b\|$	0.4482 (1)	0.477 (4)
	$\|c\|$	3.434 (4)	3.4076 (6)
S_1	$\|a\|$	0.3707 (5)	0.115 (3)
	$\|b\|$	0.3727 (5)	0.411 (4)
	$\|c\|$	3.400 (4)	3.380 (4)

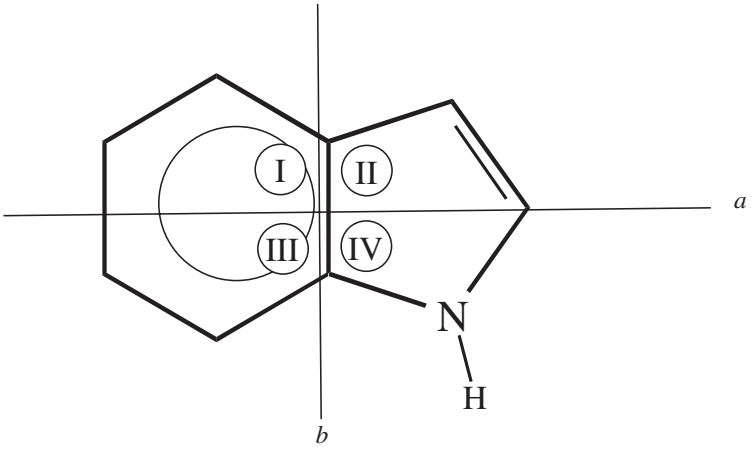

Figure 8. Two-dimensional projections of the geometry of the indole-argon van der Waals complex, as determined from a Kraitchman analysis. The four possible positions of the argon atom listed in table 4 are shown as circles. Only site IV is consistent with the results on N-deuterated-indole-argon.

excitation. But in 7AI-Ar, $|b|$ is significantly larger than $|a|$ in both states, and $|a|$ increases in the S_1 state, whereas $|b|$ decreases. The substantial differences in the coordinates of the Ar atom in the two complexes provide compelling evidence that their intermolecular PES's are different, as well.

Before discussing these differences, we first address the sign ambiguities in the two coordinates, $|a|$ and $|b|$. Each coordinate could be either positive or negative, since the moments of inertia (upon which the Kraitchman analysis is based) depend on the squares of the displacements of the different atoms from the three inertial axes. In the case of IN-Ar, this means that there are four possible binding sites, shown in figure 8. Two of the sites (I and III) are displaced toward the six-membered ring, and two of the sites (II and IV) are displaced toward the five-membered ring; site IV is nearest to the ring nitrogen atom. Fortunately, the four sites can be distinguished by deuterating the N–H hydrogen, recording and analysing the high-resolution spectrum of N-deuterated IN-Ar, using Kraitchman's equations [13] to determine the COM coordinates of the N–H hydrogen atom, in IN-Ar, and comparing these coordinates to theoretical ones. This comparison led to a clear choice of site IV as the preferred binding site [17]. The Ar atom in IN-Ar is localized above the five-membered ring, displaced toward the nitrogen atom.

We can understand this result as being a consequence of an additional attractive interaction between the Ar atom and the nitrogen lone pair electrons, which occupy an out-of-plane π-type orbital perpendicular to the ring. Calculations suggest that the S_1–S_0 electronic transition of indole results in significant charge displacement from the five-membered ring to the six-membered ring, which accords with recent measurements of the dipole moments of indole in its S_0 and S_1 electronic states (*vide infra*). This explains, then, why the magnitudes of $|a|$ and $|b|$ in IN-Ar decrease when the photon is absorbed, a 'motion' that is responsible for the observed axis tilting in its spectrum.

$|a|$ and $|b|$ are different in 7AI-Ar because the intermolecular forces are different. Figures 9 and 10 show minimum energy paths along the *a* axis of the PES's of

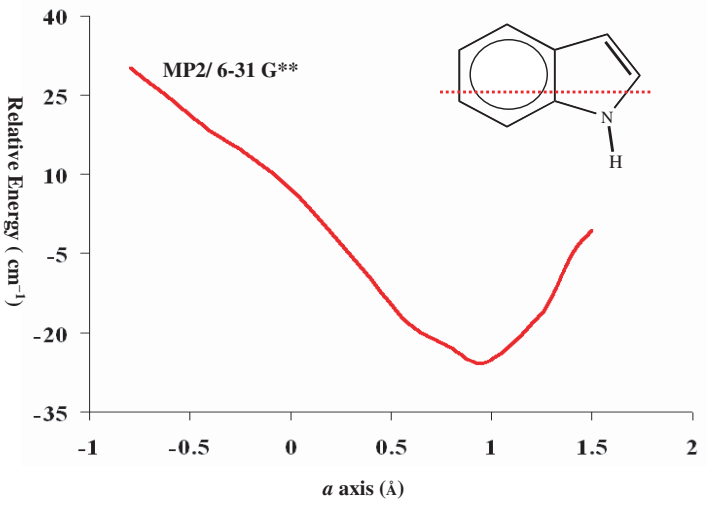

Figure 9. Potential profile of the intermolecular PES in the S_0 state of indole-argon along the minimum energy path.

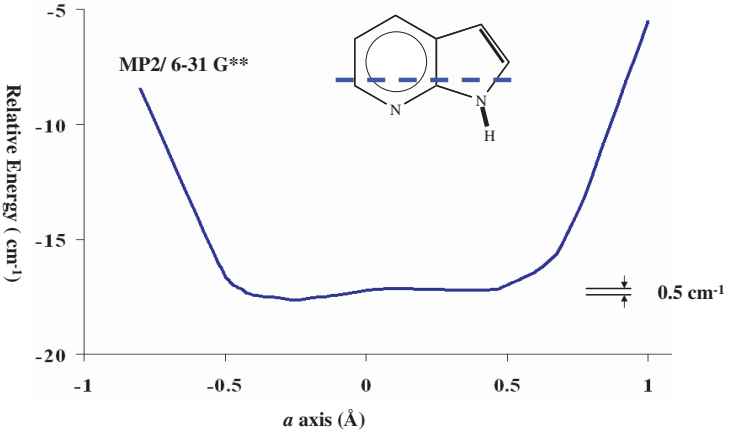

Figure 10. Potential profile of the intermolecular PES in the S_0 state of 7-azaindole-argon along the minimum energy path.

IN-Ar and 7AI-Ar calculated using MP2/6-31G** methods [15]. Both surfaces have two non-equivalent minima, at $\{-0.30, -0.45\,\text{Å}\}$ and $\{0.85, -0.45\,\text{Å}\}$ in IN, and at $\{-0.30, -0.45\,\text{Å}\}$ and $\{0.45, -0.45\,\text{Å}\}$ in 7AI. But the differences in energy between these two minima are very different in the two complexes. In IN-Ar, the minimum with positive a is at $\sim 50\,\text{cm}^{-1}$ lower energy than the minimum with negative a, giving a preferred binding site for the Ar atom that is shifted away from the centre of the two-ring system and towards the nitrogen atom in the five-membered ring. In contrast, the energy difference between one side of this system and the other in 7AI is very small. The barrier separating the two minima is very low, of order $1\,\text{cm}^{-1}$, and is barely seen on the scale of the figure, meaning that the Ar atom is not localized on either ring. The vibrationally averaged probability density is spread out

along the a axis with a maximum $\langle a^2 \rangle^{1/2}$ value near zero, in excellent agreement with the Kraitchman analysis result.

The main source of attraction that is responsible for the minima in these surfaces is likely to be a dipole-induced dipole interaction between the bare molecule and the Ar atom. IN and 7AI are apparently very different in this respect. While the two host molecules have comparable dipole moments in their ground states, 1.903 D in IN [22] and 1.45 D in 7AI [23], the orientations of these two dipoles are quite different. The dipole moment in IN is oriented along the N–C axis towards the six-membered ring ($\theta_d = 45.5^\circ$). The dipole moment in 7AI is also oriented towards this ring but points towards the ring nitrogen ($\theta_d = -24.1^\circ$). The nitrogen lone pair in the six-membered ring in 7AI apparently makes a large contribution to this dipole. Thus, while there is only one attractive nitrogen atom in IN-Ar, there are two attractive nitrogen atoms in 7AI-Ar, which leads to a delocalization of the Ar atom. The Ar atom spends most of its time in between the two local minima.

Recent Stark-effect measurements have shown that electronic excitation of 7AI leads to large changes in both the magnitude and orientation of its dipole moment; μ_a increases by 53% and μ_b decreases by 15% in the S_1 state, compared to the ground state [23]. The 0.03 Å (31%) increase in $|a|$ and 0.07 Å (14%) decrease in $|b|$ in the Ar complex of 7AI are likely consequences of this light-induced change in electronic distribution.

A wide variety of other rare gas complexes of organic molecules have been studied using high-resolution techniques. These include fluorene-Ar [24], *trans*-stilbene-Ar [25], triphenylamine-Ar [26], 1- and 2-fluoronaphthalene-Ar [14], aniline-Ar [27, 28], 4-fluorostyrene-Ar [29], pyrazine-Ar [30], 1- and 3-methylindole-Ar [31], and tetracene-Ar [32]. In aniline-Ar [27], it was found that the Ar atom resides at a distance of ~3.5 Å above the aromatic plane, and that this distance decreases slightly on excitation to the S_1 state. Additionally, the Ar atom exhibits significant large-amplitude motion in both states. Despite this fact, it remains localized on one side of ring; the *anti* structure is more stable. Thus, the symmetric double well along the inversion coordinate in aniline itself is converted into an asymmetric double well by the attachment of the Ar atom. At higher energies, aniline-Ar (and other weakly bound complexes) undergoes vibrational predissociation (VP). Their high-resolution spectra have been shown to exhibit line broadenings and spectral perturbations from which the time-scales and the important role of IVR in promoting the VP process have been elucidated [27].

2.2. *N_2 complexes*

2.2.1. *p*DFB-N_2. Figure 11 shows the rotationally resolved S_1–S_0 fluorescence excitation spectrum of the N_2 van der Waals complex of *p*DFB [33]. This spectrum differs from that of the bare molecule in three ways. First, the origin band is redshifted by ~27 cm^{-1} with respect to that of *p*DFB itself. Second, the band types of the two spectra differ. Whereas the bare molecule exhibits a pure *b*-type spectrum, showing no central Q branch, the spectrum of *p*DFB-N_2 exhibits an obvious Q branch and follows *c*-type selection rules. Both of these effects were observed in *p*DFB-Ar. But *p*DFB-N_2 exhibits a new feature not encountered before: its S_1–S_0 origin band is split into two subbands,

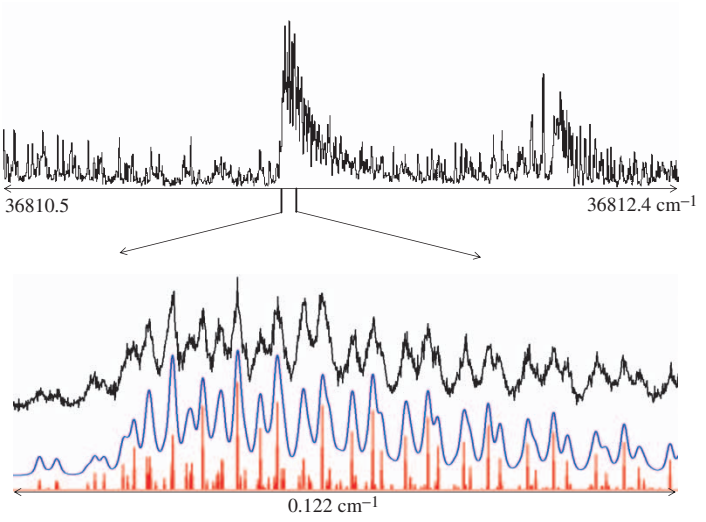

Figure 11. Rotationally resolved fluorescence excitation spectrum of the *p*-difluorobenzene-dinitrogen complex. The top trace shows the overall experimental spectrum. The bottom traces show a $\sim$0.1 cm^{-1} portion of the experimental spectrum and two simulations, with and without a superimposed lineshape function [33].

with a relative intensity of 2:1. The electronic origin of the bare molecule (and its Ar complex) consists of only a single band.

Fitting spectra like this has provided many new challenges in high-resolution electronic spectroscopy. The effective Hamiltonian is significantly more complicated than a rigid rotor one. On the other hand, the larger numbers of parameters that are needed to describe such spectra provide more information about the molecule, its complex, and the forces that hold it together. In the particular case of *p*DFB-N_2, the 'new' motion that is revealed by this spectrum is a hindered internal rotation of the attached N_2. Thus, if such a spectrum can be fitted, we learn a great deal about the anisotropy of the intermolecular potential. This is what makes small molecules like N_2, H_2O, NH_3, and CH_4 interesting binding partners in the van der Waals (and hydrogen bonded) complexes of organic molecules.

The Hamiltonian that governs the internal motion of the attached N_2 is

$$\hat{H}^{t}_{eff} = Fp^2 + (V_2/2)(1 - \cos 2\tau) \tag{2}$$

Here, F is the reduced rotational constant for the motion described by the angle τ, p is the angular momentum of the N_2 rotor, and V_2 is an effective hindering potential. (The same Hamiltonian would be used to describe the motion of a two-fold rotor like an OH group covalently bound to an aromatic molecule.) A single rotor of this type has two torsional levels for each torsional quantum number v, a single A torsional level and a single B torsional level. Degenerate in the infinite barrier limit, the two levels are split by tunnelling through a finite barrier. A similar situation exists in both electronic states. However, since their barriers are likely to be different, the tunnelling splitting will be different, and the allowed electronic transitions (A–A and B–B) also will be split, by the difference in the tunnelling splitting in the two electronic states. This is why

the spectrum of *p*DFB-N_2 is split into two subbands. Each subband, in turn, is described by different rotational constants, since the *A* and *B* torsional levels sample different regions of the potential along this coordinate.

Fortunately, there is one other interaction that influences the spectra of such species, and that is the torsion-rotation interaction. As is apparent, torsions possess (a partially quenched) angular momentum, and this couples to the corresponding angular momentum associated with overall rotational motion. A detailed discussion of this coupling, first analysed in detail by Herschbach [34], may be found in the monograph by Gordy and Cook [35]. Suffice it to state here that one can determine the axis about which the motion is occurring, its orientation in the molecular frame, and the barrier to internal rotation in both electronic states by carefully measuring such couplings in a high-resolution spectrum. We have written elsewhere about several applications of this method to isolated molecules [36, 37].

Unfortunately, it has so far proven impossible to fit the weaker of the two subbands in Figure 11. However, more than 200 lines in the stronger subband have been fitted to high precision (OMC = 4.4 MHz) when centrifugal distortion terms are included [11]. Information about the geometry of the complex was obtained from its planar moments of inertia (*P*). There are related to the ordinary moments of inertia (*I*) by $P_a = (I_a + I_b - I_c)/2$, etc. Values of these for both *p*DFB and *p*DFB-N_2 are listed in table 5.

In the bare molecule, the *c* inertial axis is perpendicular to the ring plane and the *a* inertial axis lies in this plane, passing through the fluorine atoms. Examining the data in table 5, we see that P_a (*p*DFB-N_2) ($=P_a$) $\approx P_a$ (*p*DFB) ($=P_a^m$). This means that the orientation of the *a* axis in *p*DFB is unchanged on complexation. We also see that $P_c \approx P_b^m$. This means that the orientation of the *b* and *c* axes are exchanged when the N_2 is attached, thus explaining why the 0_0^0 band of *p*DFB–N_2 is *c* axis polarized. The S_1–S_0 TM of the complex still lies in the plane of *p*DFB, approximately perpendicular to *a*.

Table 5 also lists values of the differences in the relevant planar moments of *p*DFB-N_2 from which more structural information can be obtained. Thus, among the

Table 5. Moments of inertia *I* and planar moments of inertia *P* of *para*-difluorobenzene (*p*DFB) and its nitrogen complex.[a]

		*p*DFB		*p*DFB-N_2	
State	Parameter	I^m	P^m	*I*	*P*
S_0	*a*	89.64 (1)	353.91 (2)	370.3 (1)	353.1(10)
	b	353.91 (2)	89.64 (2)	447.9 (2)	275.5 (10)
	c	443.55 (4)	0.00 (2)	628.7 (20)	94.8 (10)
	a–a^m			280.8 (1)	−0.8 (7)
	b–c^m			4.5 (2)	275.5 (11)
	c–b^m			274.7 (20)	5.1 (10)
S_1	*a*	95.66 (1)	352.28 (2)	363.1 (1)	353.1 (10)
	b	352.38 (2)	95.56 (2)	448.8 (2)	266.0 (10)
	c	447.83 (4)	0.10 (2)	617.8 (19)	97.1 (10)
	a–a^m			267.5 (1)	−0.6 (10)
	b–c^m			1.0 (1)	265.9 (11)
	c–b^m			265.4 (19)	1.5 (10)

[a]All values in uÅ^2. Uncertainties in the last digits are given in parentheses.

differences, $P_b - P_c^m$ is by far the largest. A large $P_b - P_c^m$ ($P_c^m \approx 0$) requires that the N_2 molecule lies on the top (or the bottom) of the benzene ring, in both electronic states. A complex configuration with the N_2 molecule lying in or near the plane of *p*DFB would require $P_b \approx 0$ and *a*- and/or *b*-type selection rules. Of further interest are the values of $P_a - P_a^m$ and $P_c - P_b^m$. Though small, neither of these planar moment differences is zero. This means that the N_2 molecule cannot be attached to *p*DFB 'end-on', perpendicular to the complex *ac* plane. Instead, the N_2 molecule must lie more or less in a plane parallel to the *ac* plane. This is a surprising result, since N_2 is roughly spherical. Its in-plane and out-of-plane polarizabilities must be substantially different.

The value of the moment of inertia of the N_2 molecule is 8.5 u Å^2 [38]. Neither planar moment difference in *p*DFB-N_2 is as large as this, but $P_c - P_b^m = 5.1$ u Å^2 and $P_a - P_a^m = -0.8$ u Å^2 in the S_0 state. The fact that these values are substantially different suggests that the N_2 molecule has a preferred orientation in *p*DFB-N_2; the N≡N axis is roughly parallel to the complex *c* axis in this state, perpendicular to the line joining the two fluorine atoms. $P_c - P_b^m$ is significantly smaller in the S_1 state, being approximately equal (in magnitude) to $P_a - P_a^m$. This suggests that the preferred orientation of the N≡N axis changes when the photon is absorbed.

A more rigorous treatment of this problem requires that the effects of large-amplitude motion be taken into account. Two types of motion would seem to be important, 'radial' motions and 'angular' motions. Radial motions result in displacements of the N_2 molecule's COM from its equilibrium position. Angular motions result in tilts of the N_2 molecule's N≡N bond axis with respect to its equilibrium position. Both types of motion should be fast on the time-scale of overall molecular rotation. Thus, the measured rotational constants are vibrationally averaged values over both kinds of coordinates.

Previous studies of the dynamical properties of similar complexes in the gas phase suggest that the intermolecular potential energy surface is relatively steep along the radial coordinate, and relatively flat along the angular ones. The same would be expected to be true for *p*DFB-N_2 [39]. Therefore, radial motions are ignored in what follows. Angular motions are taken into account by defining the coordinates ρ and τ shown in figure 12. ρ is a 'tilt' angle that describes the orientation of the N≡N axis in the *ab* plane ($\rho = 90^\circ$ in the parallel configuration), and τ is a 'torsional' angle that describes the orientation of the N≡N axis in the *ac* plane ($\tau = 0^\circ$ when the N≡N axis is parallel to the *a* axis). Using these coordinates, a set of equations can be written that describe the relations between the moments and products of inertia of the complex $I_{\alpha\alpha'}$ ($\alpha, \alpha' = a, b, c$) and those of the bare molecule I_α^m. These are [33]:

$$I_a = I_a^m + (\sin^2\tau \sin^2\rho + \cos^2\rho) I_{N_2} + \mu(b^2 + c^2) \tag{3}$$

$$I_b = I_c^m + \sin^2\rho I_{N_2} + \mu(a^2 + c^2) \tag{4}$$

$$I_c = I_b^m + (\cos^2\tau \sin^2\rho + \cos^2\rho) I_{N_2} + \mu(a^2 + b^2) \tag{5}$$

$$I_{ab} = -\cos\tau \sin\rho \cos\rho I_{N_2} - \mu ab \tag{6}$$

$$I_{ac} = -\sin\tau \cos\tau \sin^2\rho I_{N_2} - \mu ac \tag{7}$$

$$I_{bc} = -\sin\tau \sin\rho \cos\rho I_{N_2} - \mu bc \tag{8}$$

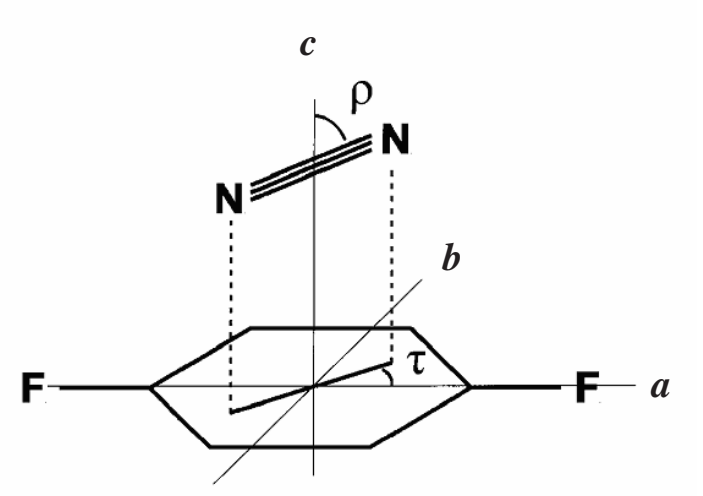

Figure 12. Geometry of the *p*-difluorobenzene-nitrogen complex. The position of the centre of mass of N_2 is defined in the principal axis system (a, b, c) of the bare *p*DFB molecule; the orientation of N_2 is defined by ρ (angle between the molecular axis of N_2 and the c axis), and τ (angle of rotation of N_2 around the c axis). The figure assumes that this axis is perpendicular to the plane.

Here, $\mu = m_{N_2} m_{DFB}/(m_{N_2} + m_{DFB}) = 22.4839$ u is the reduced mass of the complex and a, b, and c are the COM coordinates of the attached N_2 molecule in the principal axis system of the bare molecule (cf. figure 12). The potential $V(\tau)$ should be two-fold symmetric given the likely electronic distribution of *p*DFB in both states. (Only a motion that interchanges the nitrogen nuclei can explain the observed 2:1 intensity ratio between the two subbands in the UV spectrum.) Hence, averaging over τ should result in zero values for $\langle a \rangle$ and $\langle c \rangle$; the COM of the attached N_2 should lie on b. Similarly, the average values of $\langle \sin \tau \rangle$ and $\langle \cos \tau \rangle$ also should be zero. Thus, since I_{ab}, I_{ac}, and I_{bc} (equations 6–8) are zero, I is diagonal.

We now use equations (3–5) to obtain estimates of $\langle a^2 \rangle$, $\langle b^2 \rangle$, $\langle c^2 \rangle$, ρ, and τ in both electronic states. Unfortunately, there is not enough information to determine all of these parameters independently. So, we first treat the attached N_2 as a point particle with mass μ and ignore its moment of inertia I_{N_2}. Equations (3–5) then reduce to the familiar equations of Kraitchman [13]. Comparisons of the experimental moments I_a, etc. of the complex with the corresponding moments I_a^m, etc. of the bare molecule then yield estimates of the mean square displacements $\langle a^2 \rangle$, $\langle b^2 \rangle$, and $\langle c^2 \rangle$ of the COM of the attached N_2 in both electronic states. These are listed in table 6. Examining these data, we see that $\langle c^2 \rangle^{1/2} = 3.53$ Å in the S_0 state and $\langle c^2 \rangle^{1/2} = 3.45$ Å in the S_1 state. The decrease in $\langle c^2 \rangle^{1/2}$ in the S_1 state is consistent with the redshift of the S_1–S_0 origin band of *p*DFB-N_2 relative to the bare molecule; N_2 is more strongly bound in the S_1 state. The values of $\langle a^2 \rangle^{1/2}$ are relatively small and the values of $\langle b^2 \rangle^{1/2}$ are relatively large, in both electronic states. Previous studies of rare-gas complexes of aromatic molecules have yielded vibrationally averaged in-plane coordinates that are more nearly equal, as in 1-fluoronaphthalene-Ar and 2-fluoronaphthalene-Ar [14]. In contrast, *p*DFB-N_2 exhibits very different values of the two coordinates,

Table 6. Mean square displacements in Å of the nitrogen molecule in the COM coordinate system of *p*DFB in *p*DFB-N_2, in its S_0 and S_1 electronic states.[a]

Coordinate[a]	S_0	S_1
$\langle a^2\rangle^{1/2}$	0.09 (2)	0.08 (2)
$\langle b^2\rangle^{1/2}$	0.69 (2)	0.35 (2)
$\langle c^2\rangle^{1/2}$	3.53 (1)	3.45 (1)

[a]Uncertainties in parentheses.

$\langle a^2\rangle^{1/2} = 0.09$ Å and $\langle b^2\rangle^{1/2} = 0.69$ Å in the S_0 state. These data suggest that the N_2 molecule moves with significantly larger amplitude (or has significantly greater spatial extent) along b than along a, which again supports the idea that it is preferentially oriented along b, rather than a. The value of $\langle b^2\rangle^{1/2}$ is much smaller in the S_1 state. (Interestingly, $\langle a^2\rangle^{1/2}$ and $\langle b^2\rangle^{1/2}$ in the S_1 state of *p*DFB-N_2 are nearly the same as the corresponding values in *p*DFB-Ar, table 2.) All of these values are subject to some uncertainty, given the poorly defined potentials along the intermolecular coordinates. But they have at least some quantitative significance.

Next, we re-express equations (3–5) in terms of the planar moment differences $P_a - P_a^{\mathrm{m}}$, $P_b - P_c^{\mathrm{m}}$, and $P_c - P_b^{\mathrm{m}}$, obtaining

$$P_a - P_a^{\mathrm{m}} = \tfrac{1}{2}(1 + \langle\cos 2\tau\rangle)\sin^2\rho I_{\mathrm{N}_2} + \mu\langle a^2\rangle \tag{9}$$

$$P_b - P_c^{\mathrm{m}} = \cos^2\rho I_{\mathrm{N}_2} + \mu\langle b^2\rangle \tag{10}$$

$$P_c - P_b^{\mathrm{m}} = \tfrac{1}{2}(1 - \langle\cos 2\tau\rangle)\sin^2\rho I_{\mathrm{N}_2} + \mu\langle c^2\rangle \tag{11}$$

Finally, we compare the experimental values of $P_a - P_a^{\mathrm{m}}$, $\langle a^2\rangle$, etc. (tables 5 and 6) with equations (9–11), thereby obtaining estimates of $\langle\rho\rangle$ and $\langle\tau\rangle$. Equation (10) yields $\langle\rho\rangle = 45 \pm 10^\circ$ in the S_0 state and $\langle\rho\rangle = 65 \pm 15^\circ$ in the S_1 state. Apparently, the N_2 molecule spends a significant amount of time in near-perpendicular orientations, especially in the ground state. Equations (9) and (11) yield $\langle\tau\rangle = 70 \pm 10^\circ$ in the S_0 state. The corresponding value in the S_1 state is not well determined. Equation (9) gives a similar value, but equation (11) gives a value much less than this, $\langle\tau\rangle = 15 \pm 10^\circ$. We conclude, then, that the N_2 molecule lies mainly in the plane, parallel to the c axis in the S_0 state, but rotates more freely in the S_1 state.

The above analysis is deficient in two respects. First, it neglects possible contributions to B from the torsional motion itself. Second, it neglects possible contributions to $\langle a^2\rangle$, $\langle b^2\rangle$, and $\langle c^2\rangle$ from the moment of inertia of the attached N_2. A more rigorous treatment of these problems has been given by Schäfer [40].

Estimates of the barriers to internal motion in *p*DFB-N_2 may be obtained in the following way. First, we assume that the N_2 molecule is rigidly attached to *p*DFB with its N≡N axis lying in a plane parallel to the *ac* plane. We further assume that N_2 exhibits a hindered rotation about the c axis which is governed by a two-fold potential, $V_2(\tau)$. In that event, $\rho = 90^\circ$, $\langle a^2\rangle = \langle b^2\rangle = 0$, and $B_{\mathrm{rigid}} = \hbar^2/(2h[I_c^{\mathrm{m}} + I_{\mathrm{N}_2}])$, from equation (4).

The difference between this 'rigid-body' value of B and the observed B_{eff} can then be used to estimate V_2 via the relation [41]

$$B_{\text{eff}} - B_{\text{rigid}} = FW_{\text{A}}^{(2)}\left(\frac{I_{\text{N}_2}}{I_c^{\text{m}} + I_{\text{N}_2}}\right)^2 \tag{12}$$

where F is the internal rotor constant

$$F = \frac{\hbar^2}{2hI_{\text{N}_2}}\left(\frac{I_c^{\text{m}} + I_{\text{N}_2}}{I_c^{\text{m}}}\right) = 60.78\,\text{GHz} \tag{13}$$

and W_A^2 is a second-order perturbation coefficient. In the high-barrier approximation, this coefficient can be related to the energy difference between the two lowest torsional states, ΔE [41]:

$$W_A^2 = -\frac{1}{2}\pi^2 w_1 \approx \frac{1}{4}\pi^2(b_2 - b_1) = \frac{1}{4}\pi^2\frac{\Delta E}{F} \tag{14}$$

from which the reduced barrier height,

$$s = \frac{4V_{\text{N}}}{(N^2F)} \tag{15}$$

can be derived. This simple model yields $s = 6.10$ and $V_2 = 12.4\,\text{cm}^{-1}$ for the S_0 state, and $s = 3.77$ and $V_2 = 7.6\,\text{cm}^{-1}$ for the S_1 state. More refined models [40] give the estimates $\sim 10\,\text{cm}^{-1}$ and $\sim 2\,\text{cm}^{-1}$. These estimates reproduce the observed separation of the two subbands in the spectrum, ~ 21.3 GHz, showing that they are at least approximately correct.

That the N≡N bond axis is more or less uniquely oriented along the short in-plane axis in the ground state is easily rationalized. *p*DFB and N_2 are both quadrupolar molecules, owing to their high symmetry; their first non-vanishing multipole moments are the quadrupole moments, as shown below. Clearly, the stable configuration of the S_0 state of *p*DFB-N_2 should be the one in which the N_2 is attached to the top (or the

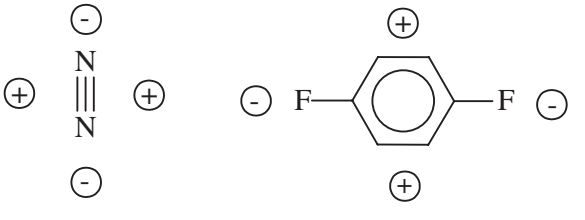

bottom) of the aromatic plane, perpendicular to the two C–F bonds. This is exactly what is observed. Further, as we have seen in an analysis of the data for *p*DFB-Ar (*vide supra*, p. 8), the quadrupole tensor of *p*DFB is less anisotropic in the S_1 state of

*p*DFB (cf. table 3 and figure 4). Thus, when *p*DFB is excited by light, the π-electron distribution in the ring becomes more isotropic, V_2 decreases, and there is no longer a preferred orientation of N_2 in the plane. Thereby manifest in a comparison of the results for *p*DFB-Ar and *p*DFB-N_2 are changes in the intermolecular potential that occur when the weakly bound species itself becomes less symmetric.

The situation in *p*DFB-N_2 stands in sharp contrast to that in aniline-N_2 [42]. Here, a large increase in barrier height is observed on S_1–S_0 excitation, from $\sim$25 cm^{-1} in the S_0 state to $\sim$65 cm^{-1} in the S_1 state. But N_2 is bound by a dipole–induced dipole interaction in aniline-N_2, leading to an equilibrium geometry in both states in which the N$\equiv$N bond axis is parallel to the *long* axis of the ring. Excitation of aniline to its S_1 state increases its dipole moment [43], thus explaining the large increase in V_2.

2.3. *Water complexes*

Due to the important role of water as a solvent and its ability to form hydrogen bonds with other molecules, either as a proton donor or acceptor, water-containing complexes have attracted a lot of attention in recent years, especially water complexes of aromatic molecules [44, 45]. If the aromatic molecule contains a functional group with oxygen or nitrogen, it normally forms a water complex with a σ hydrogen bond. In phenol-H_2O [46–48], the water binds as proton acceptor to the hydroxy group, whereas it binds as proton donor to the oxygen of the methoxy group in anisole-H_2O [49–51]. In aniline-H_2O, the water acts as proton donor to the amino group with a hydrogen bond almost perpendicular to the ring plane [52], whereas in the nitrogen-containing heterocycles pyrrole-H_2O [53] and indole-H_2O [54, 55], the water forms a N–H- - -OH_2 hydrogen bond as a proton acceptor.

Other water binding motifs exist in aromatic molecules. In the water complex of the non-polar, hydrophobic benzene molecule, water binds with its hydrogens pointing towards the π electron system, although large-amplitude motions make the elucidation of the exact structure difficult [56–60]. In complexes with more than one water molecule, the water molecules form a cluster which is hydrogen bonded to the π electron system of benzene [49, 56, 61, 62]; and in the benzene–water cation, the oxygen atom of water approaches the $C_6H_6^+$ cation in the aromatic plane, an arrangement that is about 160 cm^{-1} lower in energy than the 'a-top' geometry [63].

2.3.1. *p*DFB-H_2O. We focus on two water-containing systems here, *p*DFB-H_2O (*p*DFBW) and IN-H_2O (IW). Figure 13 shows the high-resolution electronic spectrum of the *p*DFBW complex [64]. This band is blueshifted by 168.1 cm^{-1} relative to the origin band of the bare molecule. It also contains an underlying subband structure; there are two overlapping bands in the spectrum that are separated by 3.63 GHz (0.121 cm^{-1}), as determined by an autocorrelation method. They also have different relative intensities (1:3), with the weaker subband being shifted to lower frequency. The different intensities have their origin in the nuclear spin statistical weights of the rotational levels in the complex. The two hydrogens of the attached water molecule are being exchanged by a motion that renders them equivalent, on a time-scale that is fast compared to overall rotation. The fact that the weaker subband lies to

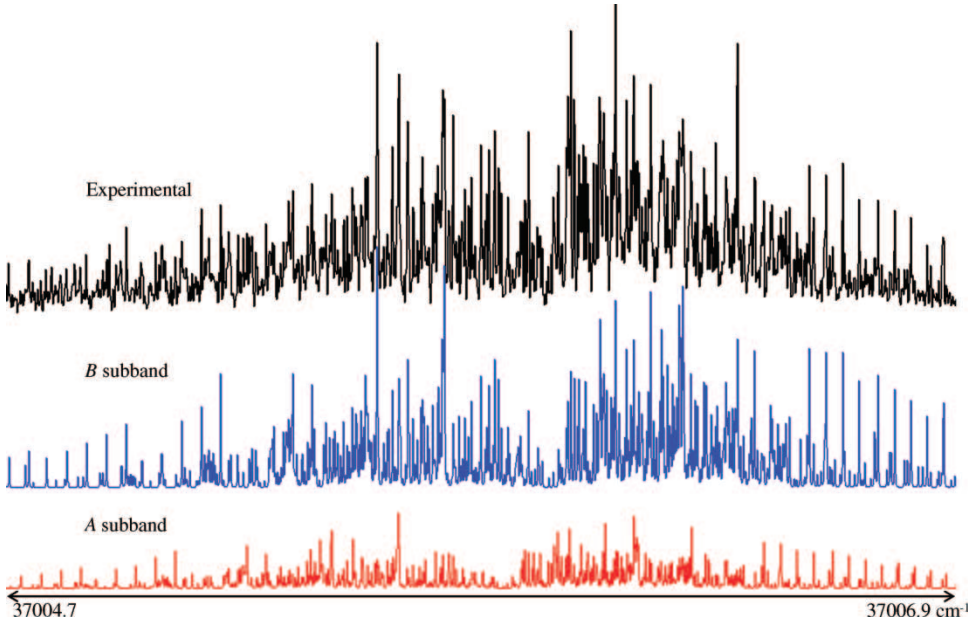

Figure 13. Rotationally resolved fluorescence excitation spectrum of the origin band of the $S_1 \leftarrow S_0$ transition of the *p*-difluorobenzene-water complex, shifted 168.1 cm^{-1} to the blue of the S_1–S_0 origin band of the bare molecule. The origin band of the complex is a superposition of two subbands that are separated by 0.121 cm^{-1}. The top trace is the experimental spectrum. The second and third traces are the calculated *B* and *A* subbands, respectively [64].

lower frequency reveals that the barrier to this motion in the excited state is less than that in the ground state. We shall return to this important point later.

We initially worked to fit the stronger of these two subbands. The fitting procedure began with the simulation of a spectrum using assumed geometries of the complex. We assumed that the water lies in the plane of *p*DFB and that one O–H bond of the water is involved in the formation of a six-membered ring system with the F–C–C–H fragment of *p*DFB, as shown in figure 14. The simulated spectrum was compared with the experimental spectrum and several transitions were assigned. An effective way to fit the spectrum is using the 'selected quantum number' feature of jb95 [12]. Each of the resolved lines was first assigned with $K_a = 0$ and subsequently followed by $K_a = 1, 2, 3, \ldots$, because the intensity significantly decreases as K_a increases. A least-squares fit of assigned quantum numbers to the spectrum with the procedure outlined above was used to modify the assumed rotational constants. This procedure was repeated iteratively until all stronger lines were accounted for. To fit the weaker band, a second spectrum was generated using the rotational constants of the stronger subband and moved along the frequency axis based on the autocorrelation results. A selected K_a quantum number assignment was carried out in the manner described above and optimized by a least-squares fit. This fit is shown in figure 15. Table 7 lists the inertial parameters that were determined in this way.

Inertial defects (ΔI) are often used as measure of a molecule's planarity. For a rigid planar structure, ΔI is zero whereas for a rigid non-planar structure, ΔI is negative.

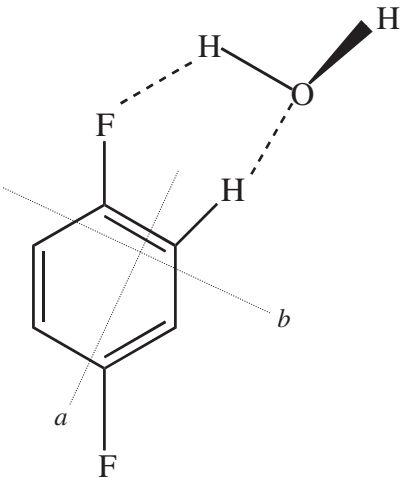

Figure 14. Approximate structure of the doubly hydrogen-bonded complex of *p*-difluorobenzene with a single water molecule. *a* and *b* denote its in-plane inertial axes.

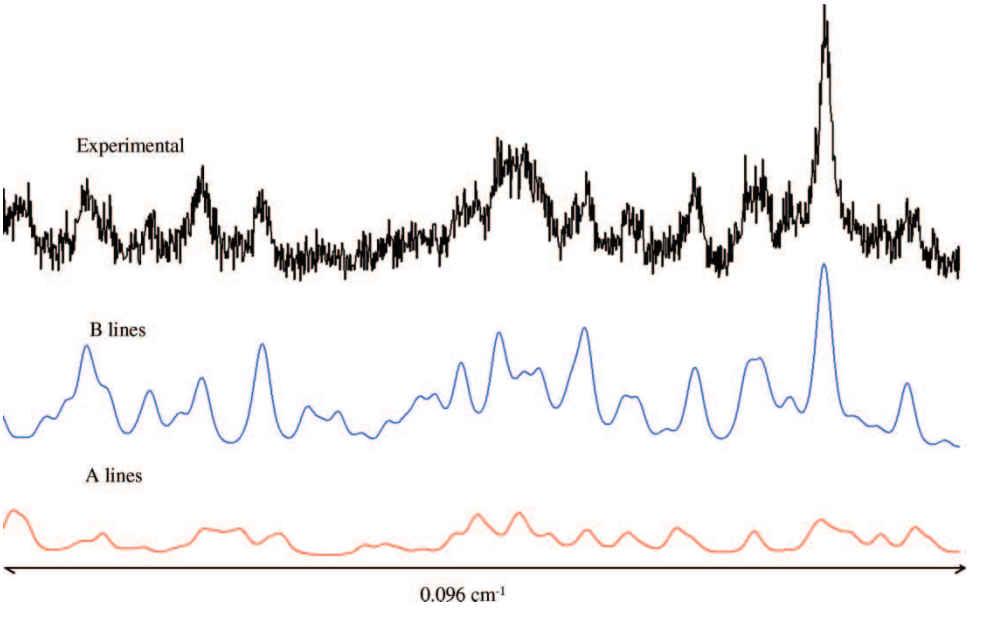

Figure 15. Portion of the high-resolution spectrum of *p*-difluorobenzene-water at full experimental resolution, extracted from the *R* branch of the stronger subband. The top trace is the experimental spectrum. The second and third traces show the separate calculated contributions of the two subbands in this region [64].

Concerning *p*DFBW, the magnitude of its inertial defects are relatively small ($\Delta I'' = -0.68\,\mathrm{u\,\AA^2}$ in the ground state and $\Delta I' = -0.74\,\mathrm{u\,\AA^2}$ in the excited state), but significantly different from those of bare molecule ($\Delta I'' = 0.00(5)\,\mathrm{u\,\AA^2}$, $\Delta I' = -0.020(5)\,\mathrm{u\,\AA^2}$) [10]. But the values for *p*DFBW are lower than that expected for two

Table 7. Inertial parameters of the water complex of pDFB in the zero-point vibrational levels of its S_0 and S_1 electronic states.

		*p*DFB-H_2O	
State	Parameter	*A* subband	*B* subband
S_0	A, MHz	3310.0 (2)	3309.6 (2)
	B, MHz	806.1 (1)	806.1 (1)
	C, MHz	648.7 (1)	648.8 (1)
	ΔI, uÅ	−0.68	−0.68
S_1	A, MHz	3185.1 (2)	3184.6 (2)
	B, MHz	795.4 (1)	795.5 (1)
	C, MHz	637.1 (1)	637.1 (1)
	ΔI, uÅ	−0.80	−0.74

out-of-plane hydroxy hydrogen atoms. For comparison, the IW complex exhibits an inertial defect of $\Delta I'' = -1.41\,\mathrm{u\,\AA^2}$ in the ground state [54]. This is about twice *p*DFBW's value. The differences are mainly explained by out-of-plane vibrational motions of the two hydrogens in water. Indole itself is essentially planar in both electronic states, and both water hydrogens are out-of-plane in the complex. While it is difficult to reach structural conclusions based on the results for a single isotopomer, the data for *p*DFBW suggest that, on average, the oxygen atom and one hydrogen atom of the water molecule lie in the plane, and the second hydrogen atom lies out-of-plane. Both hydrogens undergo large-amplitude motion along out-of-plane coordinates.

More information about the structure of the complex and the possible motions of the water molecule can be deduced from the Kraitchman analysis [13] shown in table 8. This analysis gives the position of the COM of the attached molecule from a comparison of the moments of inertia of the bare molecule and the complex. The relatively small, non-zero $|c|$ values in both electronic states are due to the out-of-plane motions of the two hydroxy hydrogen atoms. The in-plane displacements $|a| = 3.605$ and $|b| = 2.85\,\mathrm{\AA}$ in the ground state increase on electronic excitation by $0.05 - 0.10\,\mathrm{\AA}$. An increase in these distances is consistent with a decreasing strength of the two hydrogen bonding interactions, which is responsible for the blueshift of the origin band of the water complex relative to that of the bare molecule.

It is interesting to compare the results for *p*DFBW to those for the analogous benzonitrile–water (BNW) complex [65–68]. In both complexes, the oxygen is bound

Table 8. Centre-of-mass (COM) coordinates in Å of the water molecule in the principal axis frames of the bare *p*DFB molecule and of the *p*DFB-H_2O complex.

State	Coordinate	*p*DFB frame	Complex frame
S_0	$\|a\|$	3.605 (5)	3.848 (7)
	$\|b\|$	2.858 (4)	1.132 (3)
	$\|c\|$	0.23 (3)	0.067 (9)
S_1	$\|a\|$	3.703 (5)	3.916 (8)
	$\|b\|$	2.905 (3)	1.107 (2)
	$\|c\|$	0.24 (3)	0.065 (10)

to an *ortho* hydrogen and one hydroxy hydrogen is bound to the fluorine or the cyano group. In the ground state, the structures of these complexes are very similar. The water COM in BNW is slightly further away from the aromatic ring (coordinates with respect to the ring centre; 3.59/3.14/0.00 Å). However, *p*DFBW and BNW differ in their behaviour in the electronically excited state. Whereas there is no significant change in the *a* and *b* centre-of-mass coordinates in BNW (they decrease by less than 0.01 Å), the coordinates increase by $0.05-0.10$ Å in *p*DFBW. The larger structural change in *p*DFBW is also reflected in the larger blueshift of the origin of the complex with respect to that of the monomer; 168.1 cm^{-1} in *p*DFB. In contrast, BNW exhibits a redshift of 69.8 cm^{-1} with respect to that of BN itself [68].

More specific information about the motion of the water molecule in *p*DFBW comes from an analysis of the observed tunnelling splitting of 3.63 GHz. Also, each of the subbands has slightly different rotational constants due to the coupling between the torsional motion of the water molecule and overall rotation. The differences between the rotational constants of two subbands are calculated from $\Delta A'' = A''_{vo} - A''_{v1}$, $\Delta A' = A'_{vo} - A'_{v1}$ and so forth [36]. According to table 7, the rotational constants of the two subbands of the water complex are the same to within the error limits except for the *A* values; $\Delta A'' = 0.4$ MHz in the ground state and $\Delta A' = 0.5$ MHz in the excited state. This shows that the axis about which the motion of the water molecule is primarily occurring in the two states is approximately the same, and that this axis is approximately parallel to the *a* principal inertial axis of the complex.

As discussed in the analysis of the analogous tunnelling splitting in BNW [68], there exist several possible models for the motion of the attached water molecule. All require the breaking and remaking of at least one of the hydrogen bonds (F---H–O or H---O–H). The simplest model is an internal rotation of the H_2O about its C_2-(*b*-)axis within a planar equilibrium structure. The spectrum was analysed with a semirigid internal rotor model consisting of a rigid frame with C_s symmetry and one rigid internal rotor of C_{2v} symmetry [69, 70]. For each electronic state, the molecule-fixed axis system (x, y, z) was rigidly attached to the frame with its origin at the COM of the whole molecule. The *z* axis was chosen to be parallel to the internal rotation axis, and the *y* axis was chosen to be parallel to the complex *c* principal axis, perpendicular to the symmetry plane of the frame. In a least-squares fit, the moments of inertia of the complex I_{xx}, I_{yy}, I_{zz} and the potential term V_2 of the potential for both states were determined. The planar moment of the H_2O internal rotor P_x was fixed to the value obtained from ground state rotational constant $B_0 = 435$ GHz [71]. This procedure yields upper limits for the V_2 potential barriers of $V''_2 = 450\ cm^{-1}$ and $V'_2 = 290\ cm^{-1}$. The angle θ between the internal rotation axis and the *a* principal axis of the complex was estimated to be about 70° in S_1 whereas no preferred orientation was found for S_0. This result leads to a predicted subband splitting of 3.6 GHz, in good agreement with the experimental value of 3.63 GHz. However, it is clear that the axis about which the water molecule is moving in the ground state cannot be its *b* axis because such a motion would require a breaking of the hydrogen bond, a much higher energy process than 450 cm^{-1}. With the value $\theta = 70°$ in the excited state, since the internal rotation axis also has a component along the *b* axis, the *B* rotational constant of the complex also should be perturbed. But, no differences in the *B* values of the two subbands was observed.

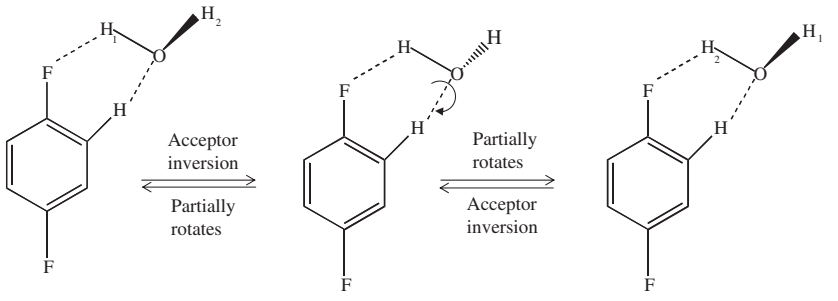

Figure 16. Combined inversion and restricted internal rotation of the water molecule in *p*DFB-H_2O.

In a second model, the water molecule was assumed to rotate about an axis in its *bc* plane, 55° off its *b* axis ($F = 339$ GHz [71]), which corresponds to a rotation about one of the lone pairs of the oxygen atom. This motion leads to barrier estimates of $V_2'' = 330 \pm 20\,\mathrm{cm}^{-1}$ in the ground state and $V_2' = 230 \pm 30\,\mathrm{cm}^{-1}$ in the excited state, with a predicted subband splitting of 3.33 ± 0.9 GHz, in good agreement with the experimental value of 3.63 GHz. However, this simple motion does not provide for the equivalent exchange of the two hydrogens, which is needed to reproduce the observed 3:1 intensity ratio.

In the third, and preferred model, the observed tunnelling splitting and differences in rotational constants are attributed the combined effects of inversion and restricted internal rotation, as shown in figure 16. This process breaks down into two visualizable steps; switching of the lone pairs by inversion and a restricted internal rotation of the water molecule. The net effect is a C_2 rotation of the water about its *b* symmetry axis. The two motions taken together are equivalent to the 'acceptor switching' motion in the H_2O dimer [2]. Importantly, the combined motion renders the two hydroxyl hydrogens equivalent, explaining the observed 3:1 intensity ratio.

In this model, the determined values of V_2 ($V_2'' = 330$ and $V_2' = 230\,\mathrm{cm}^{-1}$) are the effective barrier heights for the combined inversion-torsion motion. But we imagine that the two steps make different contributions to V_2. The barrier to water inversion in ground state *p*DFBW is likely to be relatively low, probably much less than the $130\,\mathrm{cm}^{-1}$ barrier in the water dimer [2]. In contrast, the barrier to the torsional motion of the attached H_2O in *p*DFBW is likely to be higher, owing to the stronger C–F---H–O interaction. The strength of this interaction is significantly decreased in the S_1 state; a principal reason for this decrease is the electron density redistribution in *p*DFB. As we have discussed earlier, the fluorine lone pair electron density in the S_1 state of *p*DFBW is significantly reduced, compared to the ground state, leading to a significantly reduced value of V_2 in the excited state. MP2/6-31G** calculations confirm that, in the ground state, the C–F---H–O binding energy is about $300\,\mathrm{cm}^{-1}$, whereas the C–H–O–H binding energy is much weaker, $30\,\mathrm{cm}^{-1}$ or so.

The geometry of the C–F---H–O intermolecular interaction is considerably different from those of O–H---O and O–H---N hydrogen bonds. Whereas the normal hydrogen bonding angle is almost linear, the angle C–F-H is significantly decreased to around 110° [72], making for weaker interactions. In comparison with CH_2F_2–H_2O

($\sim$700 cm^{-1}) [73], our O–H- - -F intermolecular interaction ($\sim$300 cm^{-1}, including the water inversion motion) appears to be significantly weaker. Arguably, the acceptor ability of C(sp^2)–F is not as good as that of C(sp^3)–F. Still, the strength of any hydrogen bond depends more on donor acidity than on acceptor basicity, an effect that is nicely confirmed by comparisons of the properties of the *p*DFB and BN water complexes. The V_2 barriers in BNW are nearly the same in both states [68]. There are obviously only very small changes in the electronic structure of BN upon excitation, which is also indicated by a small increase of its dipole moment in the S_1 state (+0.09 D) [74].

2.3.2. IN-H_2O (IW). Because the water molecule in *p*DFBW is linked to the substrate *p*DFB via two points of attachment (cf. figures 14 and 16), its motion (and the change in this motion when the photon is absorbed) is rather restricted. IW is different in this respect. The water molecule in IW is linked to the substrate IN molecule by only one point of attachment, an acceptor H–O- - -H–N hydrogen bond. Other motions then become feasible, including possible changes in both the position and the orientation of the attached water molecule. Such a 'solvent reorganization' is an important concept in the condensed phase. In what follows, we briefly review what has been learned about this phenomenon from high-resolution electronic spectroscopy experiments in the gas phase.

Figure 17 shows the rotationally resolved fluorescence excitation spectrum of the origin band of the S_1–S_0 transition of IW, shifted by 132 cm^{-1} to the red of the corresponding band of indole itself [54]. Again we find two subbands in the spectrum, a consequence of a tunnelling motion of the attached water molecule. The two subbands again have an intensity ratio of 1:3, with the weaker subband being shifted to the red; the subband separation is 0.444 cm^{-1} (13.3 GHz) in this case. Fits of these two subbands also showed that there are small but significant differences in the inertial parameters of the two subbands, as in the case of *p*DFBW. These results are shown in table 9.

A Kraitchman analysis [13] of these data shows that the water molecule is attached to the indole frame via a *quasi*-linear N–H- - -OH_2 hydrogen bond with the water plane more or less perpendicular to the indole plane. The COM distance of the water molecule from the indole frame also decreases by $\sim$0.1 Å when the photon is absorbed, reflecting an increase in the strength of the hydrogen bond in the S_1 state, compared to the ground state. This is consistent with the observed redshift of 132 cm^{-1}. But the most interesting light-induced motion of the attached water molecule is a change in its orientation in the S_1 state, compared to the ground state.

Examining the data in table 9, we see that only the A'' values of the two ground state subtorsional levels are different ($\Delta A'' = 1.69 \pm 0.25$ MHz), whereas both the A' values and the B' values of the two excited state subtorsional levels are different ($\Delta A' = 1.27 \pm 0.27$, $\Delta B' = 0.59 \pm 0.31$ MHz). This shows that the axes about which the motion of the water molecule is occurring in the two states cannot be the same.

Two limiting models have been developed to deal with this problem, summarized in table 10. In the first, the motion of the water molecule is assumed to be a simple rotation about its *b* axis, with an internal rotor constant of 435 GHz in both electronic states of the complex [71]. Then, using the principal axis method in the high-barrier approximation [36], we estimate from the observed differences in the rotational constants of

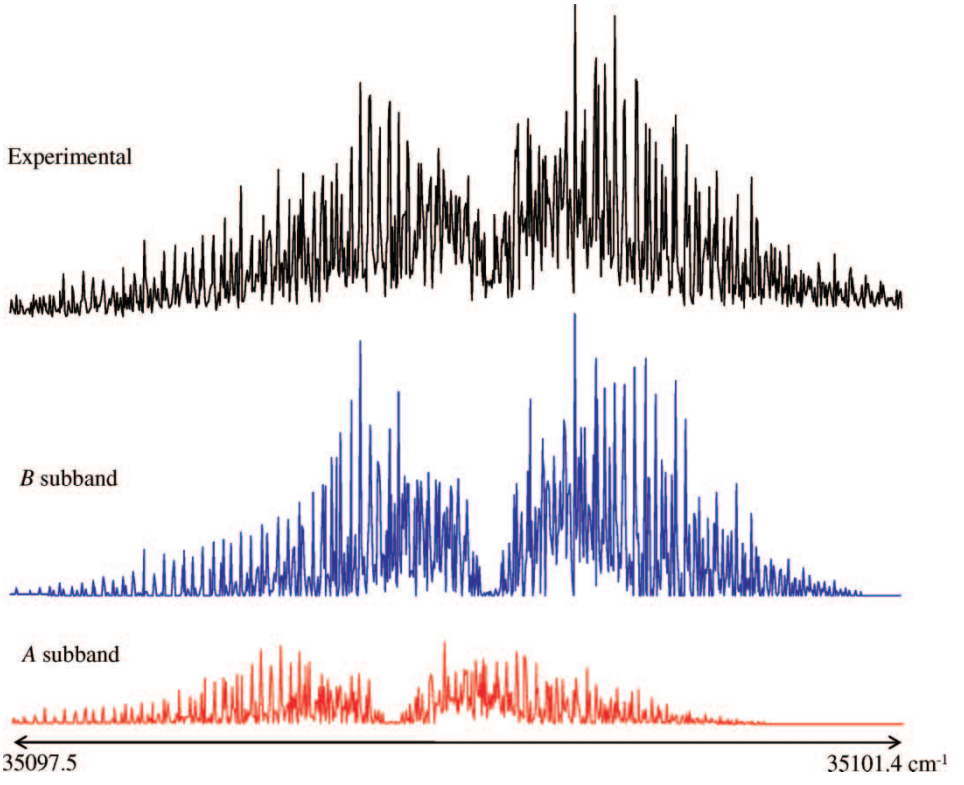

Figure 17. Rotationally resolved fluorescence excitation spectrum of the origin band of the S_1–S_0 transition of indole-water, shifted 132 cm^{-1} to the red of the S_1–S_0 origin band of indole. The origin band of the complex is a superposition of two subbands which are separated by 0.4441 cm^{-1}. The top trace is the experimental spectrum. The second and third traces are the calculated *B* and *A* subbands, respectively [54].

Table 9. Inertial parameters of the indole water complex in the zero-point vibrational levels of its S_0 and S_1 electronic states.

		Indole-H_2O	
State	Parameter	*A* subband	*B* subband
S_0	A, MHz	2064.2 (2)	2062.5 (1)
	B, MHz	945.0 (3)	945.1 (1)
	C, MHz	649.2 (2)	649.3 (1)
	ΔI, uÅ	−1.142	−1.412
S_1	A, MHz	1989.0 (2)	1987.6 (1)
	B, MHz	964.1 (3)	963.5 (1)
	C, MHz	650.4 (2)	650.4 (1)
	ΔI, uÅ	−1.249	−1.745

the two subtorsional levels a rotor axis angle (with respect to the *a* axis of the complex) of $\theta = 0^\circ$ and a barrier height of $V_2 = 198\,cm^{-1}$ in the ground state. The corresponding values in the excited state are $\theta = 55^\circ$ and $V_2 = 140\,cm^{-1}$. This leads to a predicted subband splitting of 21.319 GHz, in poor agreement with the experimental value of

Table 10. Internal rotation calculations on indole-H_2O.

State	Parameter	Rotation about water's *b* axis	Rotation about an axis in the *bc* plane, 55° off the *b* axis
S_0	Rotor constant (GHz)	435.352	339.277
	θ (°)	0±15	0±15
	V_2 (cm^{-1})	198.2±14.0	168.5±12.0
	Subtorsional splitting (GHz)	15.273±3.021	9.276±2.000
S_1	Rotor constant (GHz)	435.352	339.277
	θ (°)	55±15	55±15
	V_2 (cm^{-1})	140.1±25.0	121.7±20.0
	Subtorsional splitting (GHz)	36.592±13.550	22.2232±8.231

13.314 GHz. In the second model, the water molecule is assumed to rotate about an axis in its *bc* plane, 55° off the *b* axis, with an internal rotor constant of 339 GHz [71]. This model yields rotor angles of $\theta(S_0) = 0°$ and $\theta(S_1) = 55°$ as before but significantly lower values of the barriers, $V_2(S_0) = 169\,cm^{-1}$ and $V_2(S_1) = 122\,cm^{-1}$. This leads to a predicted subband splitting of 12.947 GHz, in good agreement with the experimental value. We cannot explain our data by assuming that the water internal rotation axis itself changes when the photon is absorbed (cf. table 9). Therefore, we conclude that the axis about which the water molecule is moving lies in its *bc* plane, 55° off the *b* axis, in *both* electronic states of the complex, and that the orientation of this axis relative to the *a* axis of IW changes by 55° on S_1 excitation.

Shown in figure 18 are sketches of the local solvent structures in IW in the two electronic states that are consistent with these results. Both structures have linear (or nearly linear) HB's; however, the orientation of the water plane relative to the HB axis in the two states is different. In the ground state, the N–H hydrogen is linked to one of the two sp^3 lone pairs of the oxygen atom, resulting in an angle between the water plane and the HB axis of ~55°. In the excited state, the N–H hydrogen is linked to both lone pairs, resulting in a bifurcated structure with an angle between the water plane and the HB axis of ~0°. Apparently, the observed solvent reorganization is a consequence of 'radial-angular coupling'; i.e. decreasing the heavy-atom separation R by electronic excitation produces a change in the preferred orientation of the solvent plane with respect to the HB axis. (The $-132\,cm^{-1}$ complex exhibits a short Franck–Condon progression along at least one mode, with a frequency of $24\,cm^{-1}$. Presumably, this mode is related to the structural changes reported here. See [75]).

In retrospect, it is clear that the axis about which the water molecule is moving in the ground state cannot be its *b* axis because such a motion would require a breaking of the HB, a much higher energy process than 100–200 cm^{-1}. It is also clear that the motion of the water molecule cannot be a simple torsional motion about an axis 55° off its *b* axis, since such a motion would not render the two water hydrogens equivalent. Therefore, the observed tunnelling splitting (and differences in rotational constants) must, in fact, be due to the combined effects of internal rotation and inversion, or 'wag', similar to the motion of the water molecule in *p*DFBW and phenol–H_2O [47]. This model accounts, at least in a qualitative way, for the observed out-of-plane motion of the water molecule. The derived values of V_2 are thus effective barrier heights for the torsion-inversion motion.

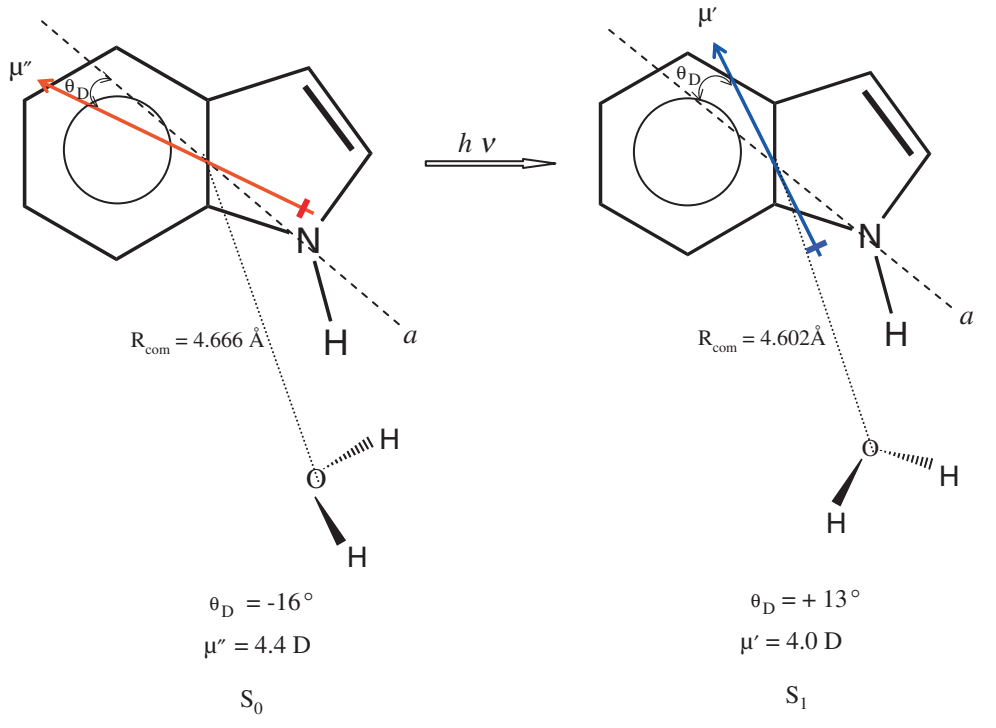

Figure 18. Indole-water showing its inertial axes and the orientations of its permanent electric dipole moments in the two electronic states.

2.3.3. Stark-effect measurements. According the time-honoured concept of solvent reorganization, solvent molecules move in response to a change in the local electronic environment produced by the absorption of light. Molecules in electronically excited states are presumed to have dipole moments whose magnitudes and orientations are different from those in the ground state. Recently, we have tested this idea by performing Stark-effect experiments on several molecules in the gas phase. In the case of indole [22], we find that $\mu = 1.963$ D in the S_0 state, and $\mu = 1.856$ D in the S_1 state. These two values are not very different. But we also find that the orientation of the permanent dipole moment changes significantly when the molecule absorbs light, by $\sim 13^\circ$, reflecting a shift in electron density from the pyrrole ring to the benzene ring. Thus, it is indeed true that the water molecule reorients when indole absorbs light because such a reorientation leads to a more favourable relative orientation of their respective dipoles (cf. figure 18). To the best of our knowledge, this is the first 'structurally resolved' and fully documented demonstration of this effect in the literature.

Being able to perform Stark-effect experiments on isolated molecules in the gas phase puts us in a unique position to determine the induced dipole moment that is produced when a solvent molecule like water is attached to a polarizable molecule like indole. Shown in figure 19 is a portion of the rotationally resolved electronic spectrum of IW and its response to an applied electric field [22]. Clearly evident are Stark-induced splittings and shifts in both the positions and intensities of the observed lines.

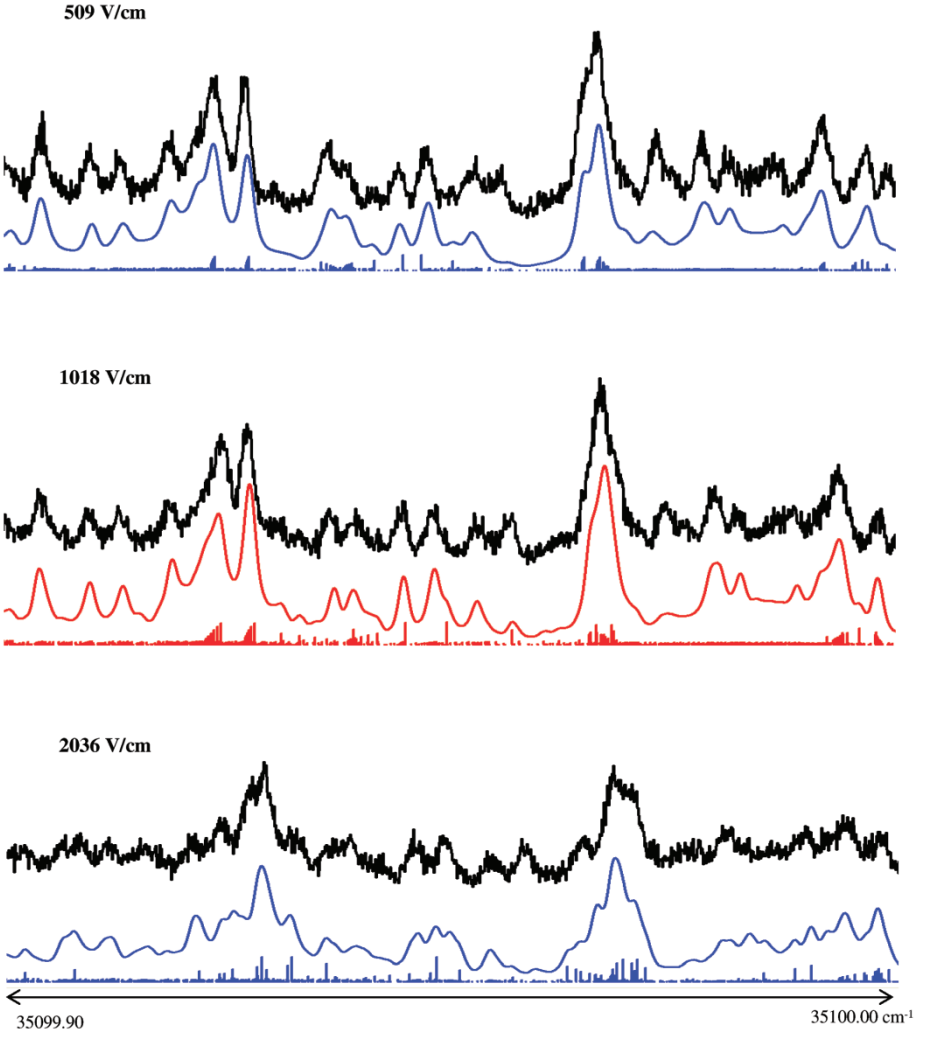

Figure 19. Portion of the rotationally resolved spectrum of indole-water extracted from near the origin of the $B' \leftarrow B''$ subtorsional band showing the influence of an applied electric field [22].

Fitting these data, it was found that the dipole moment of IW is 4.4 ± 0.3 D in the ground S_0 state and 4.0 ± 0.3 D in the excited S_1 state. Now, water in its ground state has a dipole moment $\mu_W = 1.855(6)$ D [76]. Combining this value with the measured values for indole gives maximum values for IW of 3.818 in S_0 and 3.711 D in S_1, assuming the dipoles of the component parts are aligned. The measured values of 4.4 and 4.0 D are larger than these estimates by 13% in S_0 and 8% in S_1. We attribute these differences to induced dipole moments produced by the attached water molecule.

Electrostatic models of the interactions between molecules have been successful in predicting the structure of many van der Waals complexes [77–79]. In a

typical model, the dipole moment of the complex can be represented as a sum of three terms,

$$\mu_{IW} = \mu_I + \mu_W + \mu_I^*. \tag{16}$$

Here, μ_I and μ_W are the permanent dipole moments of the component parts, for which the experimental values are now known, and μ_I^* is the induced dipole moment. This arises primarily from polarization of the indole unit by the water dipole and quadrupole moments, μ_W and Θ_W:

$$\mu_I^* = \alpha_I \cdot \left\{ \left[3\mathbf{R}(\mu \cdot \mathbf{R})/R^5 \right] - \mu/R^3 + \left[5(\mathbf{R}^\dagger \cdot \Theta \cdot \mathbf{R})/R^7 \right]\mathbf{R} - (\Theta^\dagger \cdot \mathbf{R} + \Theta \cdot \mathbf{R})/R^5 \right\} \tag{17}$$

Expressed in the inertial coordinate system of indole, equation (17) can be simplified to

$$\mu_{I\,a,b}^* \approx \mu_{W\,a,b} \frac{2\alpha_{I\,a,b}}{R_{COM}^3} + 3\Theta_{W\,a,b} \frac{\alpha_{I\,a,b}}{R_{COM}^4} \tag{18}$$

Here, $\alpha_{I\,a,b}$ is the polarizability volume of indole, and $\mu_{W\,a,b}$ and $\Theta_{W\,a,b}$ are the electric dipole and quadrupole moments of water, each referred to either the a or b inertial axis of indole. The water molecule may be assumed to lie in the ab plane of the complex since its tunnelling motion is fast compared to overall molecular rotation. R_{COM} is the COM distance between indole and water which also can be determined from experiment; the values (see figure 18) are $R_{COM} = 4.666$ and $R_{COM} = 4.602$ Å in the S_0 and S_1 states, respectively.

The polarizabilities and quadrupole moments that are needed in these calculations were obtained by *ab initio* methods using a 6-31G** basis set [15]. Predictably, these lead to large induced dipole moments whose magnitudes are strongly angularly dependent. For example, if we consider only the first (dipole) term in equation (18), we calculate a ground state induced moment of 0.567 D when the water dipole points along a and 0.346 D when the water dipole points along b. These values changes to 0.721 and 0.507 D, respectively, when indole is excited to its S_1 state. The larger induced dipole in the S_1 state may be traced to the larger polarizability and smaller R_{COM} in that state.

We now use equation (18) to determine the induced dipole moments in IW. Essentially quantitative agreement with experiment is obtained when the C_2 axis of water is oriented by -25° with respect to the a axis of the complex in the S_0 state and by $+35^\circ$ with respect to the a axis of the complex in the excited state. This is shown in table 11. The induced dipole moments in these two orientations are $\mu_I^* = 0.727$ ($\mu_{Ia}^* = 0.592$ and $\mu_{Ib}^* = 0.422$ D) in the S_0 state, and $\mu_I^* = 0.540$ ($\mu_{Ia}^* = 0.484$ and $\mu_{Ib}^* = 0.238$ D) in the S_1 state. The S_1 induced dipole is smaller by 0.187 D. Primarily, this is because the dipoles of water and indole are nearly aligned (-25.7°) in the ground state, but less well aligned ($+48.3^\circ$) in the excited state. The values of the water orientation angles required by the fit are in nearly perfect agreement with the values derived from our earlier analysis of the torsion-rotation perturbations in the high-resolution spectrum [54]. The error limits reflect a less than 2° uncertainty

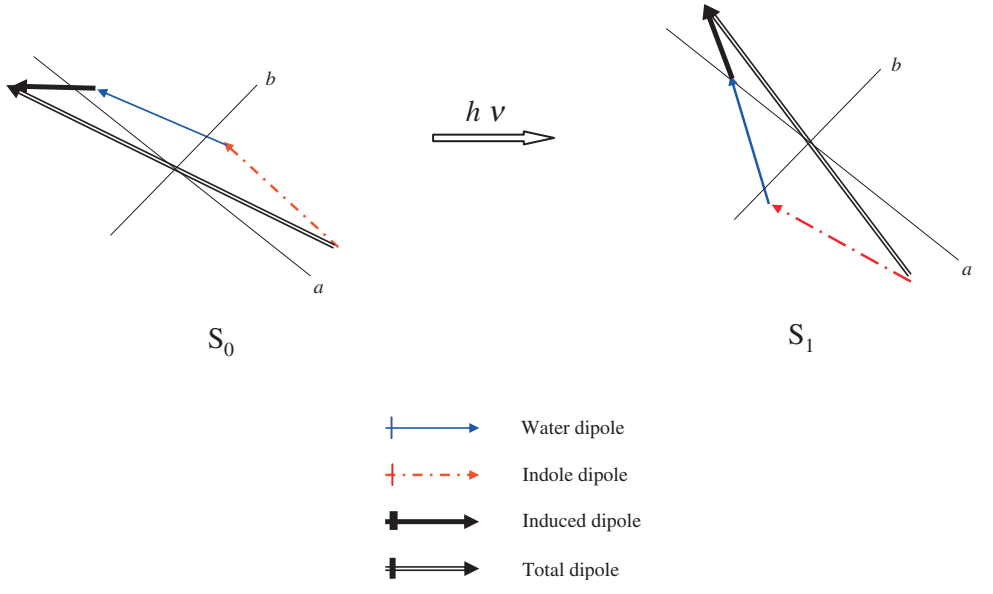

Figure 20. Illustration of the magnitudes and orientations of the permanent and induced electric dipole moments of indole-water in its S_0 and S_1 electronic states [22].

Table 11. Observed and calculated dipole moments of indole and indole–water in their S_0 and S_1 electronic states.

			Indole-Water		
				Calculated	
State	Dipole Moments	Indole	Experimental	W/O Θ	W/Θ
S_0	μ_a	1.376 (8)	4.20 (6)	4.11	4.24
	μ_b	1.40 (1)	1.2 (3)	1.15	1.18
	μ_{tot}	1.963 (13)	4.4 (3)	4.27	4.40
S_1	μ_a	1.556 (8)	3.90 (8)	3.54	3.81
	μ_b	1.01 (1)	0.9 (3)	0.66	0.77
	μ_{tot}	1.856 (13)	4.0 (3)	3.60	3.89

in the vibrationally averaged orientation of the water molecule compared to the experimental data.

Figure 20 summarizes these results in graphical form. That the polarizing effect of the water molecule would increase the dipole moment of the complex was expected owing to the high polarizability of the indole molecule. What was unexpected is the magnitude of the effect; the induced moment in IW is a substantial fraction (30–40%) of the permanent dipole moment of indole itself. The distribution of electrons in the isolated molecule is significantly affected by the presence of a single solvent molecule in its vicinity. Also unexpected is the fact that the induced dipole is not parallel to the 'inducing' one, especially in the ground state. Possibly this effect has its origin in the polarizability anisotropy, which is larger in the ground state. But most surprising of all is that

a simple electrostatic model seems to capture the essence of the polarization phenomenon so well. If this result holds up under further scrutiny, then the prospects for success of recently derived polarizable force fields for other organic and biological molecules is high [80].

3. Summary

An immense amount of information can be derived from the fully resolved electronic spectrum of an isolated large molecule and its weakly bound complexes in the gas phase. This information includes their geometries in the two electronic states 'connected' by the photon. That is, the experiment gives information about the position (and orientation) of the attached atom or molecule, and how this changes when the molecule absorbs light. Motions of the attached species along different intermolecular coordinates are revealed by perturbations in the spectrum. And, finally, the application of an externally applied field to the sample produces Stark splittings and shifts of the lines in the spectrum from which one can derive both the permanent and induced dipole moments of weakly bound complexes in both electronic states. Light-induced changes in the charge distributions of such species are often intimately linked to their changes in structure.

The particular species discussed here include Ar, N_2, and H_2O complexes of organic molecules like *p*-difluorobenzene, indole, and 7-azaindole. The interactions explored include dipole–dipole, dipole–induced dipole, and quadrupole–quadrupole interactions. Different species exhibit different structures and dynamics depending on the nature of the interactions of the component parts. Thus, symmetry (or lack of symmetry) is important. With further developments in technology, the methods of analysis described here will find many future applications in increasingly complex systems, including those in biology, thereby continuing to stimulate the refinement of our understanding of the forces between molecules in both the gas and condensed phase.

Acknowledgments

David Borst, Tim Korter, Martin Schäfer, Wayne Sinclair, and John Yi have each made major contributions to this work. We thank them all. We also are grateful to Hans-Jürgen Neusser for permission to use figure 2, Tom Shattuck and his colleagues at Colby College for their hospitality as this paper was being written, and the National Science Foundation for its support of our research (CHE-0315584) at the University of Pittsburgh.

References

[1] D. H. Levy, NATO Advanced Study Institutes Series, Series B: Physics B57 (Quantum Dynamics of Molecules), pp. 115–42 (1980).
[2] C.-J. Tsai and K. D. Jordan, Chem. Phys. Lett. **213,** 181 (1993).
[3] J. G. Gregory and D. C. Clary, J. Chem. Phys. **105,** 6626 (1996).
[4] J. B. Paul, R. A. Provencal, C. Chapo, A. Petterson, and R. J. Saykally, J. Chem. Phys. **109,** 10201 (1998).

[5] R. S. Fellers, L. B. Braly, R. J. Saykally, and C. Leforestier, J. Chem. Phys. **110,** 6306 (1999).
[6] J. M. Hutson, A. Ernesti, M. M. Law, C. F. Roche, and R. J. Wheatley, J. Chem. Phys. **105,** 9130 (1996).
[7] W. A. Majewski, J. F. Pfanstiel, D. F. Plusquellic and D. W. Pratt, in *Laser Techniques in Chemistry*, edited by A. B. Myers and T.R. Rizzo (Wiley, New York, 1995), Vol. 101, p. 23.
[8] S. Gerstenkorn and P. Luc, Atlas du spectroscopie d'absorption de la molecule d'iode, CNRS: Paris (1978 and 1982).
[9] D. G. Lister, J. K. Tyler, J. H. Høg, and N. W. Larsen, J. Mol. Struct. **23,** 253 (1974).
[10] R. Sussmann, R. Neuhauser, and H. J. Neusser, Can. J. Phys. **72,** 1179 (1994).
[11] J. K. G. Watson, in *Vibrational Spectra and Structure*, edited by J. R. Durig (Elsevier, Amsterdam, 1977), Vol. 6, p. 1.
[12] Described in D. F. Plusquellic, R. D. Suenram, B. Maté, J. O. Jensen, and A. C. Samuels, J. Chem. Phys. **115,** 3057 (2001).
[13] J. Kraitchman, Am. J. Phys. **21,** 17 (1953).
[14] B. B. Champagne, J. F. Pfanstiel, D. W. Pratt, and R. C. Ulsh, J. Chem. Phys. **102,** 6432 (1995).
[15] M. J. Frisch, G. W. Trucks, H. B. Schlegel, G. E. Scuseria, M. A. Robb, J. R. Cheeseman, V. G. Zakrzewski, J. A. Montgomery, R. E. Stratmann, J. C. Burant, S. Dapprich, J. M. Millam, A. D. Daniels, K. N. Kudin, M. C. Strain, O. Farkas, J. Tomasi, V. Barone, M. Cossi, R. Cammi, B. Mennucci, C. Pomelli, C. Adamo, S. Clifford, J. Ochterski, G. A. Petersson, P. Y. Ayala, Q. Cui, K. Morokuma, D. K.Malick, A. D. Rabuck, K. Raghavachari, J. B. Foresman, J. Cioslowski, J. V.Ortiz,B. B. Stefanov, G. Liu, A. Liashenko, P. Piskorz, I. Komaromi, R. Gomperts, R. L. Martin, D. J. Fox, T. Keith, M. A. Al-Laham, C. Y. Peng, A. Nanayakkara, C. Gonzalez, M. Challacombe, P. M. W. Gill, B. G. Johnson, W. Chen, M. W. Wong, J. L. Andres, M. Head-Gordon, E. S. Replogle and J. A. Pople, *Gaussian 98*, *Revision A9; Gaussian, Inc*. Pittsburgh, PA, (1998).
[16] R. Sussmann and H. J. Neusser, J. Chem. Phys. **102,** 3055 (1995).
[17] T. M. Korter, J. Küpper, and D. W. Pratt, J. Chem. Phys. **111,** 3946 (1999).
[18] J. T. Hougen and J. K. G. Watson, Can. J. Phys. **43,** 298 (1965).
[19] A. Held, B. B. Champagne, and D. W. Pratt, J. Chem. Phys. **95,** 8732 (1991).
[20] D. F. Plusquellic and D. W. Pratt, J. Chem. Phys. **97,** 8970 (1992).
[21] C. -H. Kang, J. T. Yi, and D. W. Pratt, submitted.
[22] C.-H. Kang, T. M. Korter, and D. W. Pratt, J. Chem. Phys., **122**, 174301 (2005).
[23] C.-H. Kang, J. T. Yi, and D. W. Pratt, submitted.
[24] W. M. van Herpen, W. L. Meerts, H. E. Hunziker, M. S. de Vries, and H. R. Wendt, Chem. Phys. Lett. **147,** 7 (1988).
[25] B. B. Champagne, D. F. Plusquellic, J. F. Pfanstiel, D. W. Pratt, W. M. van Herpen, and W. L. Meerts, Chem. Phys. **156,** 251 (1991).
[26] G. Meijer, G. Berden, W. L. Meerts, H. E. Hunziker, M. S. de Vries, and H. R. Wendt, Chem. Phys. **163,** 209 (1992).
[27] W. E. Sinclair and D. W. Pratt, J. Chem. Phys. **105,** 7942 (1996).
[28] M. Becucci, G. Pietraperzia, N. M. Lakin, E. Castellucci, and Ph. Bréchignac, Chem. Phys. Lett. **260,** 87 (1996).
[29] N. M. Lakin. G. Pietraperzia, M. Becucci, E. Castellucci, M. Coreno, A. Giardini-Guidoni, and A. van der Avoird, J. Chem. Phys. **108,** 1836 (1998).
[30] K. Remmers, R. G. Satink, G. van Helden, W. L. Meerts, H. E. Hunziker, M. S. de Vries, and H. R. Wendt, Chem. Phys. Lett. **317,** 197 (2000).
[31] T. M. Korter and D. W. Pratt, J. Phys. Chem. B **105,** 4010 (2001).
[32] I. Szydlowska, G. Myszkiewicz, and W. L. Meerts, Chem. Phys. **371,** 283 (2002).
[33] M. Schäfer, C.-H. Kang, and D. W. Pratt, J. Phys. Chem. A **107,** 10753 (2003).
[34] D. R. Herschbach, J. Chem. Phys. **27,** 975 (1957).
[35] W. Gordy and R. L. Cook, *Microwave Molecular Spectra*, 3rd ed. (Wiley Interscience, New York, 1984).
[36] X.-Q. Tan, D. F. Plusquellic, W. A. Majewski, and D. W. Pratt, J. Chem. Phys. **94,** 7721 (1991).
[37] L. H. Spangler and D. W. Pratt, in *Jet Spectroscopy and Molecular Dynamics*, edited by J. M. Hollas and D. Phillips (Chapman and Hall, Ltd., London, 1995), p. 366.
[38] A. Lofthus and P. H. Krupenie, J. Phys. Chem. Ref. Data **113,** 6 (1977).
[39] S. Lee, J. Romascan, P. M. Felker, T. B. Pedersen, B. Fernández, and H. Koch, J. Chem. Phys. **118,** 1230 (2003).
[40] M. Schäfer, Phys. Chem. Chem. Phys. **6,** 3271 (2004).
[41] D. R. Herschbach, J. Chem. Phys. **31,** 91 (1959).
[42] M. Schäfer and D. W. Pratt, J. Chem. Phys. **115,** 11147 (2001).
[43] T. M. Korter, D. R. Borst, C. J. Butler, and D. W. Pratt, J. Am. Chem. Soc. **123,** 96 (2001).
[44] B. Brutschy, Chem. Rev. **100,** 3891 (2000).
[45] K. S. Kim, P. Tarakeshwar, and J. Y. Lee, Chem. Rev. **100,** 4145 (2000).
[46] M. Gerhards, M. Schmitt, K. Kleinermanns, and W. Stahl, J. Chem. Phys. **104,** 967 (1996).

[47] G. Berden, W. L. Meerts, M. Schmitt, and K. Kleinermanns, J. Chem. Phys. **104,** 972 (1996).
[48] S. Melandri, A. Maris, P. G. Favero, and W. Caminati, Chem. Phys. **283,** 185 (2002).
[49] H. -D. Barth, K. Buchhold, S. Djafari, B. Reimann, U. Lommatzsch, and B. Brutschy, Chem. Phys. **239,** 49 (1998).
[50] M. Becucci, G. Pietraperzia, M. Pasquini, G. Piani, A. Zoppi, R. Chelli, E. Castellucci, and W. Demtröder, J. Chem. Phys. **120,** 5601 (2004).
[51] J. W. Ribblett, W. E. Sinclair, D. R. Borst, J. T. Yi, and D.W. Pratt, submitted.
[52] U. Spoerel and W. Stahl, J. Mol. Spectrosc. **190,** 278 (1998).
[53] M. J. Tubergen, A. M. Andrews, and R. L. Kuczkowski, J. Phys. Chem. **97,** 7451 (1993).
[54] T. M. Korter, D. W. Pratt, and J. Küpper, J. Phys. Chem. A **102,** 7211 (1998).
[55] J. R. Carney, F. C. Hagemeister, and T. S. Zwier, J. Chem. Phys. **108,** 3379 (1998).
[56] A. J. Gotch and T. S. Zwier, J. Chem. Phys. **96,** 3388 (1992).
[57] S. Suzuki, P. G. Green, R. E. Bumgarner, S. Dasgupta, W. A. Goddard III, and G. A. Blake, Science **257,** 942 (1992).
[58] H. S. Gutowsky, T. Emilsson, and E. Arunan, J. Chem. Phys. **99,** 4883 (1993).
[59] R. N. Pribble, A. W. Garrett, K. Haber, and T. S. Zwier, J. Chem. Phys. **103,** 531 (1995).
[60] T. Emilsson, H. S. Gutowsky, G. de Oliveira, and C. E. Dykstra, J. Chem. Phys. **112,** 1287 (2000).
[61] A. W. Garrett and T. S. Zwier, J. Chem. Phys. **96,** 3402 (1992).
[62] R. N. Pribble and T. S. Zwier, Faraday Discuss. Chem. Soc. **97,** 229 (1994).
[63] N. Solcà and O. Dopfer, Chem. Phys. Lett. **347,** 59 (2001).
[64] C.-H. Kang, D. W. Pratt, and M. Schäfer, J. Phys. Chem. A **109,** 767 (2005).
[65] R. M. Helm, H. Vogel, H. J. Neusser, V. Storm, D. Consalvo, and H. Dreizler, Z. Naturforsch. Teil A, **52,** 655 (1997).
[66] V. Storm, H. Dreizler, and D. Consalvo, Chem. Phys. **239,** 109 (1998).
[67] S. Melandri, D. Consalvo, W. Caminati, and P. G. Favero, J. Chem. Phys. **111,** 3874 (1999).
[68] M. Schäfer, D. R. Borst, D. W. Pratt, and K. Brendel, Mol. Phys. **100,** 3553 (2002).
[69] A. Bauder, E. Mathier, R. Meyer, M. Ribeaud, and H. H. Günthard, Mol. Phys. **15,** 597 (1968).
[70] M. Schäfer, J. Chem. Phys. **115,** 11139 (2001).
[71] F. C. DeLucia, P. Helminger, R. L. Cook, and W. Gordy, Phys. Rev. A **5,** 487 (1972).
[72] P. Tarakeshwar, K. S. Kim, and B. Brutschy, J. Chem. Phys. **110,** 8501 (1999).
[73] W. Caminati, S. Melandri, I. Rossi, and P. G. Favero, J. Am. Chem. Soc. **121,** 10098 (1999).
[74] D. R. Borst, T. M. Korter, and D. W. Pratt, Chem. Phys. Lett. **350,** 485 (2001).
[75] P. L. Muińo and P. R. Callis, Chem. Phys. Lett. **222,** 156 (1994).
[76] S. A. Clough, Y. Beers, G. P. Klein, and L. S. Rothman, J. Chem. Phys. **59**, 2254 (1973).
[77] K. C. Janda, L. S. Bernstein, J. M. Steed, S. E. Novick, and W. Klemperer, J. Am. Chem. Soc. **100,** 8074 (1978).
[78] R. S. Altman, M. D. Marshall, W. Klemperer, and A. Krupnov, J. Chem. Phys. **79,** 52 (1983).
[79] R. S. Altman, M. D. Marshall and W. Klemperer, J. Chem. Phys. **77,** 4344 (1982).
[80] C. S. Ewig, M. Waldman and J. R. Maple, J. Phys. Chem. A **106,** 326 (2002); J.W. Ponder *et al.*, in press.